

# GAIN VARIATION AND NOISE FIGURE DEGRADATION IN BALANCED AMPLIFIERS

A DISSERTATION SUBMITTED TO  
THE GRADUATE SCHOOL OF ENGINEERING AND SCIENCE  
OF BILKENT UNIVERSITY  
IN PARTIAL FULFILLMENT OF THE REQUIREMENTS FOR  
THE DEGREE OF  
DOCTOR OF PHILOSOPHY  
IN  
ELECTRICAL AND ELECTRONICS ENGINEERING

By  
Akif Alperen Coşkun  
July 2017

GAIN VARIATION AND NOISE FIGURE DEGRADATION IN  
BALANCED AMPLIFIERS

By Akif Alperen Coşkun

July 2017

We certify that we have read this dissertation and that in our opinion it is fully adequate, in scope and in quality, as a dissertation for the degree of Doctor of Philosophy.

---

Abdullah Atalar(Advisor)

---

Cemal Yalabık

---

Vakur Behçet Ertürk

---

Şimşek Demir

---

Barış Bayram

Approved for the Graduate School of Engineering and Science:

---

Ezhan Karaşan  
Director of the Graduate School

In reference to IEEE copyrighted material which is used with permission in this thesis, the IEEE does not endorse any of Bilkent University's products or services. Internal or personal use of this material is permitted. If interested in reprinting/republishing IEEE copyrighted material for advertising or promotional purposes or for creating new collective works for resale or redistribution, please go to [http://www.ieee.org/publications\\_standards/publications/rights/rights\\_link.html](http://www.ieee.org/publications_standards/publications/rights/rights_link.html) to learn how to obtain a License from RightsLink.

#### Copyright Information

©2017 IEEE. Reprinted, with permission, from A. A. Coskun and A. Atalar, "Noise Figure Degradation in Balanced Amplifiers", IEEE Microwave and Wireless Components Letters, accepted June 3, 2017.

# ABSTRACT

## GAIN VARIATION AND NOISE FIGURE DEGRADATION IN BALANCED AMPLIFIERS

Akif Alperen Coşkun

Ph.D. in Electrical and Electronics Engineering

Advisor: Abdullah Atalar

July 2017

Although using balanced amplifiers in modern wireless communication systems has many advantages, the output and the noise response of the balanced amplifiers may vary from the expected value considerably due to the imperfections in the amplifier and the divider/combiner sections. First, we analyze the variation in the total gain of the balanced amplifiers using 2-way  $0^\circ$  power dividers and  $90^\circ$  couplers. In this context, mathematical analyses are made and analytical expressions are obtained to compare the two topologies. Analytical expressions show that the uncertainty in the total gain is more if the  $90^\circ$  coupler is used in the balanced structure as opposed to a 2-way  $0^\circ$  power divider for the same return loss/isolation values. Then, we present exact and approximate analytical results for the noise figure and noise parameters of the balanced amplifier in divider topology by using the noise waves. By the help of the noise wave approach, the output noise powers generated by each element in the balanced amplifier are derived. Y-parameters are used to determine the noise waves and the correlation matrix of the divider whereas the noise parameters are used to write the noise waves of the amplifier. Balanced amplifiers suffer in the noise figure performance in comparison to a stand-alone amplifier even with an ideal input divider. The noise parameters degrade further with an imperfect divider. Not only the non-zero return loss and the isolation but also the ohmic loss, amplitude and phase imbalances are considered. Besides, non-zero optimal source impedance affects the noise parameters of the balanced amplifier. Measurement results are also presented as a verification.

*Keywords:* Balanced amplifiers, gain variation, mismatch, noise figure, noise parameters, noise waves, phase and amplitude imbalance, two-way dividers, hybrid couplers.

## ÖZET

# DENGELİ YÜKSELTEÇLERDE KAZANÇ VARYASYONU VE GÜRÜLTÜ FIGÜRÜ KÖTÜLEŞMESİ

Akif Alperen Coşkun

Elektrik-Elektronik Mühendisliği, Doktora

Tez Danışmanı: Abdullah Atalar

Temmuz 2017

Modern kablosuz iletişim sistemlerinde dengeli yükselteçleri kullanmak birçok avantaja sahip olmakla birlikte, yükselteçteki ve bölücü/birleştirici bölümlerdeki ideal dışı durumlar sebebiyle, dengeli yükselteçlerin kazanç ve gürültü tepkisi beklenen değerden önemli ölçüde farklı olabilir. İlk olarak, 2-kollu  $0^\circ$  güç bölücü ve  $90^\circ$  bağlaç kullanan dengeli yükselteçlerde, kazançta oluşan varyasyonları analiz ediyoruz. Bu bağlamda, iki topoloji için karşılaştırmalı olarak matematiksel analizler yapılmış ve analitik ifadeler elde edilmiştir. Analitik ifadeler göstermiştir ki, aynı geri yansıma kaybı/izolasyon değerleri için,  $90^\circ$  kuplör kullanılan dengeli yükselteçlerde toplam kazançtaki belirsizlikler 2-kollu  $0^\circ$  güç bölücü kullanıldığı duruma göre daha fazladır. Ardından, gürültü dalgalarını kullanarak, bölücülü dengeli yükselteç topolojisinin gürültü figürü ve gürültü parametreleri için kesin ve yaklaşık analitik sonuçları sunuyoruz. Gürültü dalga yaklaşımının yardımıyla, dengeli yükselteçteki her bir elemanın çıkışta ürettiği gürültü gücü çıkarılmıştır. Bölücünün ilinti matrisi ve gürültü dalgalarını belirlemek için bölücünün Y-parametreleri, yükseltecin gürültü dalgalarını yazabilmek için yükseltecin gürültü parametreleri kullanılmıştır. Dengeli yükselteçler, ideal bir giriş bölücüyle bile, tekil yükseltece kıyasla gürültü figürü performansından muzdariptir. Gürültü parametreleri, ideal olmayan bir bölücü ile daha da bozulur. Sadece sıfır olmayan dönüş kaybı ve izolasyon değil aynı zamanda omik kayıp, genlik ve faz dengesizlikleri de göz önüne alınmıştır. Ayrıca, sıfır olmayan optimum kaynak empedansı, dengeli yükseltecin gürültü parametrelerini etkilemektedir. Ölçüm sonuçları da bir doğrulama olarak sunulmuştur.

*Anahtar sözcükler:* Dengeli yükselteçler, kazanç varyasyonu, uyumsuzluk, gürültü figürü, gürültü parametreleri, gürültü dalgaları, faz ve genlik dengesizlikleri, iki-kollu bölücü, hibrit bağlaç.

## Acknowledgement

I express my appreciations to Prof. Abdullah Atalar for his guidance throughout my MS and PhD studies. Prof. Atalar has always been an inspiration to me with his brilliant mind and magnificent vision. I would like to thank Prof. Cemal Yalabık and Prof. Vakur B. Ertürk for their contributions during our research meetings. I am grateful to the other members of my dissertation committee Prof. Şimşek Demir and Prof. Barış Bayram for taking the time.

I would like to thank to METEKSAN Defense Inc. and Microwave Design Department where I gained lots of technical experience in my professional life.

Finally, I would like to express my deep love to my family, my mother Aysen, my father Diler, my brother Oğuzalp and my beloved wife Ayşegül.

# Contents

<b>1</b>	<b>Introduction</b>	<b>1</b>
<b>2</b>	<b>Gain Variation of a Balanced Amplifier</b>	<b>4</b>
2.1	Balanced Amplifier with 2-Way 0° Power Divider . . . . .	4
2.2	Balanced Amplifier with 90° Coupler . . . . .	10
2.3	Comparison of Gain Variation in Balanced Amplifiers . . . . .	15
2.4	Experimental Results for Gain Variation . . . . .	15
<b>3</b>	<b>Noise Figure Analysis of a Balanced Amplifier</b>	<b>18</b>
3.1	Noise Waves for the Balanced Amplifier . . . . .	18
3.1.1	Noise Waves for the Amplifiers . . . . .	19
3.1.2	Noise Waves for the Input and Output Dividers . . . . .	21
3.1.3	Noise Waves for the Input Source . . . . .	23
3.2	Noise Figure of a Balanced Amplifier . . . . .	24
3.2.1	Noise Figure of a Balanced Amplifier . . . . .	24
3.2.2	Amplitude and Phase Imbalance . . . . .	29
3.2.3	Non-zero $\Gamma_o$ . . . . .	33
3.2.4	Experimental Results for Noise Figure . . . . .	34
<b>4</b>	<b>Conclusion</b>	<b>38</b>

# List of Figures

2.1	A balanced amplifier using 2-way $0^\circ$ power dividers. . . . .	4
2.2	Flow graph for the balanced amplifier using divider. The dashed lines show the irrelevant arms. . . . .	6
2.3	The gain variation, $\Delta S_{21}^D $ , for a balanced amplifier with divider for various divider parameters and for amplifiers with $ \Gamma_i  = -12$ dB, $ \Gamma_o  = -6$ dB. . . . .	8
2.4	The probability density of the gain deviation of a balanced amplifier with divider of various parameters. Amplifiers have $ FR  = -10$ dB, $ \Gamma_i  = -12$ dB, $ \Gamma_o  = -12$ dB. . . . .	8
2.5	The probability density of the gain deviation of a balanced amplifier with divider of various parameters. Amplifiers have $ FR  = -10$ dB, $ \Gamma_i  = -12$ dB, $ \Gamma_o  = -6$ dB. . . . .	9
2.6	The probability density of the gain deviation of a balanced amplifier with divider of various parameters. Amplifiers have $ FR  = -2$ dB, $ \Gamma_i  = -12$ dB, $ \Gamma_o  = -6$ dB. . . . .	9
2.7	A balanced amplifier using $90^\circ$ couplers. . . . .	10
2.8	Flow graph for the balanced amplifier using coupler. The dashed lines show the irrelevant arms. . . . .	11
2.9	The gain variation in $ S_{21}^C $ for a balanced amplifier with coupler for various coupler parameters and for amplifiers with $ \Gamma_i  = -12$ dB and $ \Gamma_o  = -6$ dB. . . . .	13
2.10	The probability density of the gain deviation of a balanced amplifier with coupler of various parameters. Amplifiers have $ FR  = -10$ dB, $ \Gamma_i  = -12$ dB, $ \Gamma_o  = -12$ dB. . . . .	13



2.11 The probability density of the gain deviation of a balanced amplifier with coupler of various parameters. Amplifiers have  $|FR| = -10$  dB,  $|\Gamma_i| = -12$  dB,  $|\Gamma_o| = -6$  dB. . . . . 14

2.12 The probability density of the gain deviation of a balanced amplifier with coupler of various parameters. Amplifiers have  $|FR| = -2$  dB,  $|\Gamma_i| = -12$  dB,  $|\Gamma_o| = -6$  dB. . . . . 14

2.13 The photo of the dividers, amplifiers and some of the SMA line extenders used for balanced amplifier's gain and power reduction measurements. . . . . 17

2.14 The theoretical and measured gain reduction in balanced amplifier versus transmission-line length between the amplifiers and the dividers. The measured gain variation is consistent with the theoretical calculations. . . . . 17

3.1 A balanced amplifier built using 2-way  $0^\circ$  power dividers. . . . . 19

3.2 The representation of a noisy amplifier by noise waves. . . . . 19

3.3 The flow graph of the balanced amplifier built using lossless ideal power dividers. . . . . 20

3.4 The representation of a noisy three-port network by current sources. 22

3.5 The noise figures of single and balanced amplifiers with perfect dividers as a function of source reflection coefficient. Amplifiers have  $F_m=1$  dB,  $\Gamma_o=0$  and various  $r_n$  and  $|\Gamma_i|$  values. The noise figure of a balanced amplifier is degraded in comparison to a single amplifier for the same source return loss. . . . . 26

3.6 The noise figure degradation of balanced amplifiers with perfect dividers as a function of  $F_m$ . Amplifiers have  $|\Gamma_i|=-7$  dB,  $|\Gamma_s|=-10$  dB,  $\Gamma_o=0$  and various  $r_n$  values. . . . . 26

3.7 The maximum value of the divider  $|\Gamma_r|$  to limit the noise figure degradation in the balanced amplifier with 2-way dividers to 0.1 dB for  $\Gamma_s=0$ . The amplifiers have  $|\Gamma_i|=-7$  dB . . . . . 27

3.8 The worst-case noise figure as a function of source reflection coefficient for a balanced amplifier. The input divider has an ohmic loss of 0.1 dB, and return loss and isolation better than 20 dB, 26 dB or 32 dB. The amplifiers have  $|\Gamma_i|=-7$  dB,  $F_m=1$  dB,  $r_n = 0.1$  and  $\Gamma_o=0$ . . . . . 30

3.9 The noise figure degradation as a function of the return loss and isolation for a balanced amplifier. The input divider has an ohmic loss of 0.1 dB, and  $|\Gamma_s|=-10$  dB. The amplifiers have  $|\Gamma_i|=-7$  dB,  $F_m=1$  dB,  $\Gamma_o=0$  and various  $r_n$  values. . . . . 30

3.10 Noise figure degradation with respect to the amplitude imbalance. The amplifiers have  $|\Gamma_i|=-7$  dB,  $F_m=1$  dB,  $r_n = 0.1$  and  $\Gamma_o=0$ . . . 31

3.11 Noise figure degradation with respect to the phase imbalance. The amplifiers have  $|\Gamma_i|=-7$  dB,  $F_m=1$  dB,  $r_n = 0.1$  and  $\Gamma_o=0$ . . . . . 32

3.12 S-parameters of the  $D_1$  having poor  $|\Gamma_r|$  plotted with respect to the frequency. . . . . 35

3.13 S-parameters of the  $D_2$  having good  $|\Gamma_r|$  plotted with respect to the frequency. . . . . 35

3.14 Photo of the amplifiers, divider pairs and SMA line extenders used to build balanced amplifiers. . . . . 36

3.15 Calculated (solid) and measured (points)  $F_{md}$  and  $r_{nd}$  for the balanced amplifiers  $B_1$  (circle),  $B_2$  (cross),  $B_3$  (square) and  $B_4$  (plus). The graphs show the good agreement between the theoretical and measurement results. . . . . 37

3.16 Calculated (solid) and measured (points)  $\Gamma_{od}$  for the balanced amplifiers on the Smith chart in the frequency range 1.5–1.6 GHz. The measured values of  $\Gamma_{od}$  are equal to the measured values of  $\Gamma_r^*$ , confirming our theory. . . . . 37

# List of Tables

2.1	S-Parameters in dB magnitude-angle format measured at 1.55 GHz for amplifiers . . . . .	16
2.2	S-parameters measured for both dividers at 1.55 GHz in dB magnitude-angle format. . . . .	16
3.1	Measured parameters for amplifiers $A_1/A_2$ (GALI-84+) and $A_3/A_4$ (PGA-103+) at 1.55 GHz. . . . .	34

# Chapter 1

## Introduction

Amplifiers are one of the most critical elements used in wireless communication systems where the small noise figure and high output power or gain are the common requirements. Low noise amplifiers (LNAs) and power amplifiers (PAs) are used to meet these requirements. Obtaining a small noise figure for LNAs or maximum power for PAs with good input/output return loss values at the same time may not be possible using a single amplifier. Adding an isolator in front of the LNA [1] or after the PA [2] solve the return loss problem. Balanced configuration [3,4] is widely used for amplification due to its remarkable advantages. Ideally, balanced amplifiers conserve the noise figure of the single amplifier and double the output power compared to a single-ended amplifier, while input/output return losses, linearity and stability are improved [5–13], gain of the single amplifier is preserved [2,3,14] and a redundancy is provided. While a balanced amplifier has many desirable properties, the output or the noise response of the balanced amplifiers may vary from the expected value considerably due to non-ideal components [3].

Power combining structures have been implemented using different combiner topologies, such as Wilkinson power combiner, branch-line coupler and radial combiners [15–20]. The degradations occurring at the output of the combining section are very critical for PAs. There are several papers which examine the

output behavior of the combining structures such as the output power degradation [21–26] and the combining efficiency [27–30] for different cases. Some papers examine the output behavior of the balanced amplifier configuration with the non-ideal amplifier or divider/combiner properties. Kurokawa [4] gives the overall gain formula for the balanced structure when the coupling of the directional coupler is 3 dB or different than 3 dB for identical amplifiers. Besides, the gain expression is given for non-identical amplifiers. But, the coupler is assumed to be ideal for these analyses. Another work [31] analyzes the overall transfer function of the amplifier-combiner circuit for  $N$ -way radial and planar divider/combiner and  $N$  identical amplifiers using binomial matrix expansion with truncation. However, the transfer function is complex and obtained for the perfect matching case at the  $N$ -ports for the  $N$ -way divider/combiner.

Several papers investigated the effect of imperfections on the noise performance of a balanced amplifier. The noise figure was given [3], assuming the amplifier gains are unbalanced. Kurokawa [4] explored the effect of the termination ports of the input/output couplers and Kerr [32] investigated the source impedance's effect on the noise figure of the balanced amplifier and stated that the output noise is affected by the magnitude of the source impedance, but not the phase. In these cases, the input and output couplers were assumed to be ideal. An analytical formula was presented [33] to find the cascaded noise figure of the differential amplifier with baluns assuming the baluns have symmetrical losses. The analysis was improved [34] by adding the phase and amplitude imbalance in each arm. But, the return loss/isolation of the baluns and return loss of the amplifiers are all assumed to be zero.

Practically, neither amplifiers nor divider/combiners have a perfect match or isolation. Gain variation or mismatch uncertainty [35] in cascaded networks due to imperfect port impedances is a well known fact. If the port reflection coefficients at the connected ports are  $\Gamma_1$  and  $\Gamma_2$ , the mismatch uncertainty,  $MU$ , is given by [36]

$$MU_{dB} = 20 \log_{10}(1 \pm |\Gamma_1 \Gamma_2|). \quad (1.1)$$

In Chapter 2, defining the gain variation as the ratio of maximum gain to minimum gain, we analyze the gain variation for balanced amplifiers built with imperfect two-way  $0^\circ$  dividers/combiners and hybrids ( $90^\circ$  couplers). Using the derived expressions we determine the gain for such structures statistically. Moreover, a comparison is given between these two topologies in terms of the gain variation. To verify the analytical expressions we derived, amplifier-divider pairs are designed to construct a balanced amplifier and the gain variation is obtained experimentally.

In Chapter 3, by using the noise wave approach, we analytically obtained the noise powers for each element in the balanced amplifier. The noise waves and the correlation matrix for the divider are written from its Y-parameters and the noise waves for the amplifiers are written in terms of their noise parameters. We investigate the noise figure of a balanced amplifier and find the conditions under which the noise figure is degraded compared to a stand-alone amplifier. We investigated the effect of both ideal and non-ideal dividers on the noise figure. For non-ideality, not only the imperfect return loss and the isolation but also the ohmic loss, amplitude and phase imbalance are taken into consideration. Besides, the non-zero optimal source impedance is analyzed. We present approximate noise parameters for the balanced amplifier and verify the results with experiments [37].

# Chapter 2

## Gain Variation of a Balanced Amplifier

### 2.1 Balanced Amplifier with 2-Way $0^\circ$ Power Divider

Fig. 2.1 shows a balanced amplifier constructed with two identical 2-way  $0^\circ$  power dividers and two identical amplifiers. The S-parameters of the lossless, symmet-

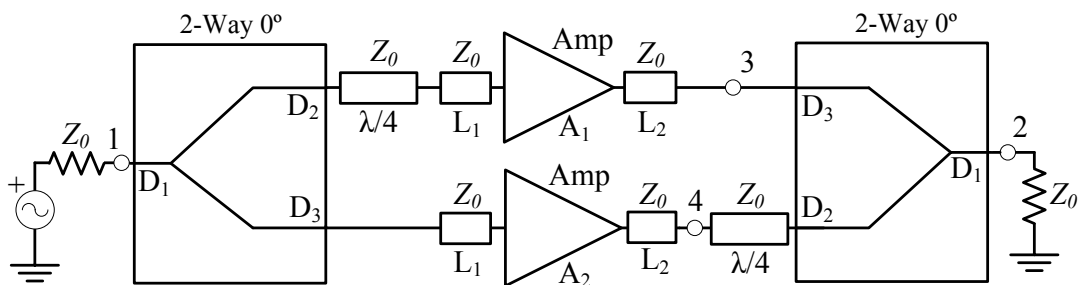


Figure 2.1: A balanced amplifier using 2-way  $0^\circ$  power dividers.

rical but imperfect dividers,  $S^d$ , and the amplifiers,  $S^a$ , with respect to  $Z_0$  are

given in the matrix form as

$$S^d = \begin{bmatrix} \Gamma_c & F_c & F_c \\ F_c & \Gamma & I \\ F_c & I & \Gamma \end{bmatrix}, \quad S^a = \begin{bmatrix} \Gamma_i & R \\ F & \Gamma_o \end{bmatrix}. \quad (2.1)$$

In  $S^d$ ,  $\Gamma_c$  denotes the return loss of the port  $D_1$ ,  $\Gamma$  denotes the return losses of the ports  $D_2$  and  $D_3$ ,  $I$  denotes the isolation between the ports  $D_2$ - $D_3$  and  $F_c$  denotes the insertion loss of both from  $D_1$  to  $D_2$  and  $D_1$  to  $D_3$  of the divider. Besides,  $\Gamma_i$  denotes the input return loss,  $\Gamma_o$  denotes output return loss,  $F$  denotes gain and  $R$  denotes the reverse isolation of the amplifier as given in  $S^a$ . Nonzero  $\Gamma$  and  $I$  of the divider may have arbitrary phases. Since the divider is lossless when excited from port 1, we have

$$|\Gamma_c|^2 + |F_c|^2 + |F_c|^2 = 1 \quad \text{and} \quad |\Gamma_c| = |\Gamma + I|, \quad (2.2)$$

where the last equality is derived in [38]. Hence we find

$$|F_c| = \frac{\sqrt{1 - |\Gamma + I|^2}}{\sqrt{2}}. \quad (2.3)$$

We note that the S-parameters of the amplifier,  $S^a$ , given in (2.1) include the phase shifts due to input ( $L_1$ ) and output ( $L_2$ ) interconnection transmission lines of arbitrary length.

Consider the signal flow-graph of the circuit shown in Fig. 2.2. Here,  $a_i$  represents the incident wave and  $b_i$  represents the reflected wave at the port  $i$ . If  $V_i$  and  $I_i$  are the *rms* voltage and current at port  $i$ , we define these quantities as

$$a_i = \frac{1}{2} \left( \frac{V_i}{\sqrt{Z_0}} + I_i \sqrt{Z_0} \right), \quad b_i = \frac{1}{2} \left( \frac{V_i}{\sqrt{Z_0}} - I_i \sqrt{Z_0} \right). \quad (2.4)$$

Using Mason's [39] rule<sup>1</sup>, we find [40] the forward gain of the balanced amplifier as

$$|S_{21}^D| = \left| \frac{b_2}{a_1} \right| = |2FF_c^2| \frac{|1 + (FR - \Gamma_i\Gamma_o)(\Gamma - I)^2|}{|\Delta_D|}, \quad (2.5)$$

---

<sup>1</sup>The flow graph has 12 forward paths, 18 loops, 21 non-touching loop pairs, eight non-touching loop triplets and a single non-touching loop quadruplet.



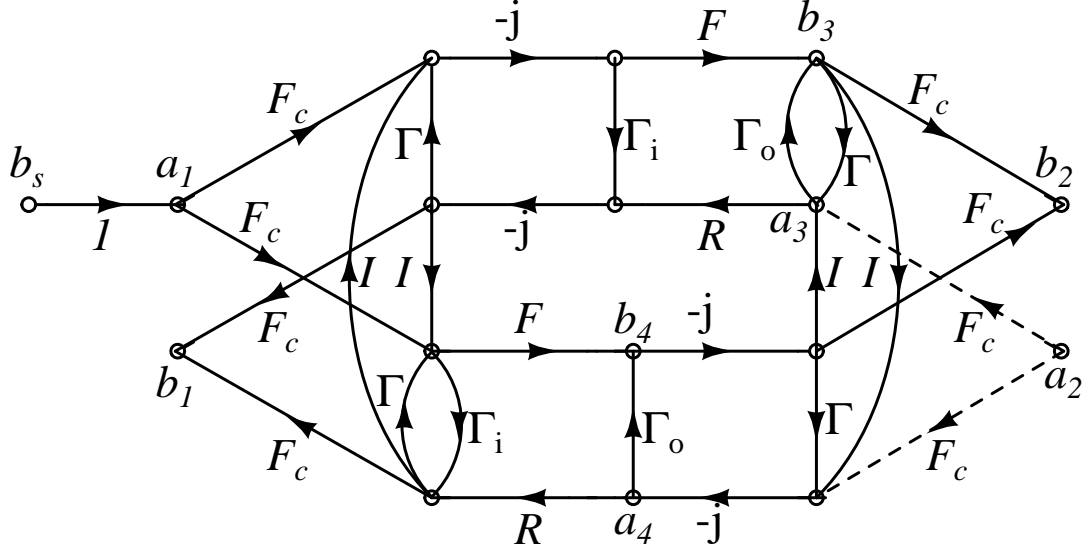


Figure 2.2: Flow graph for the balanced amplifier using divider. The dashed lines show the irrelevant arms.

where

$$\Delta_D = 1 + (\Gamma^2 + I^2)(2FR + \Gamma_i^2 + \Gamma_o^2) - 2\Gamma^2(\Gamma_i^2 + \Gamma_o^2) + (\Gamma^2 - I^2)^2(FR - \Gamma_i\Gamma_o)^2. \quad (2.6)$$

Ignoring the higher order terms, the result simplifies to

$$|S_{21}^D| \approx |2FF_c^2| \frac{|1 + FR(\Gamma - I)^2|}{|1 + 2FR(\Gamma^2 + I^2)|}. \quad (2.7)$$

For the special case of  $\Gamma = -I$  (or from the last equality of (2.2),  $|\Gamma_c|=0$ ), we get the nominal gain of

$$|S_{21}^D| \approx |F|. \quad (2.8)$$

Due to arbitrary length of interconnecting transmission lines and random phases of  $\Gamma$  and  $I$ ,  $|S_{21}^D|$  may deviate from its nominal value. It is maximized if  $\Gamma$  and  $I$  are out of phase and  $FR(\Gamma^2 + I^2) = -|FR(\Gamma^2 + I^2)|$  is negative real:

$$|S_{21}^D|_{max} \approx |F| [1 - (|\Gamma| - |I|)^2] \frac{1 - |FR|(|\Gamma| - |I|)^2}{1 - 2|FR|(|\Gamma|^2 + |I|^2)} \quad (2.9)$$

and it is minimized if  $\Gamma$  and  $I$  are of the same phase and  $FR(\Gamma^2 + I^2) = |FR(\Gamma^2 + I^2)|$  is positive real:

$$|S_{21}^D|_{min} \approx |F| [1 - (|\Gamma| + |I|)^2] \frac{1 + |FR|(|\Gamma| + |I|)^2}{1 + 2|FR|(|\Gamma|^2 + |I|^2)}. \quad (2.10)$$

We define the gain variation as

$$\Delta |S_{21}^D| = \frac{|S_{21}^D|_{max}}{|S_{21}^D|_{min}}. \quad (2.11)$$

Hence we find

$$\Delta |S_{21}^D| \approx \left( \frac{1 - (|\Gamma| - |I|)^2}{1 - (|\Gamma| + |I|)^2} \right) \left( \frac{1 - |FR|(|\Gamma| - |I|)^2}{1 + |FR|(|\Gamma| + |I|)^2} \right) \left( \frac{1 + 2|FR|(|\Gamma|^2 + |I|^2)}{1 - 2|FR|(|\Gamma|^2 + |I|^2)} \right). \quad (2.12)$$

By further algebraic manipulation, a simpler form is obtained with no  $|\Gamma_i|$  or  $|\Gamma_o|$  dependence as

$$\Delta |S_{21}^D| \approx \frac{1 + D - D'}{1 - D}, \quad (2.13)$$

where

$$D = (1 + |FR|)(|\Gamma| + |I|)^2 \quad (2.14)$$

and

$$D' = 2(1 + |FR|)(|\Gamma|^2 + |I|^2). \quad (2.15)$$

(2.13) is accurate to within 2%, as long as  $|FR| \leq -2$  dB,  $|\Gamma_i| \leq -8$  dB,  $|\Gamma_o| \leq -8$  dB,  $|\Gamma| \leq -16$  dB and  $|I| \leq -16$  dB.

In Fig. 2.3, the gain variation,  $\Delta |S_{21}^D|$ , is plotted using the exact expression of (2.5) for various divider parameters. The gain variation decreases with the decreasing  $|FR|$  product of the amplifier. The gain variation is also minimized, when  $|\Gamma|$  or  $|I|$  is minimized. We verified the expression in (2.5) by a linear microwave simulator.<sup>2</sup> We performed a Monte-Carlo analysis by allowing the phases of the amplifier S-parameters as well as the phases of  $\Gamma$  and  $I$  to vary randomly with a uniform distribution. Figs 2.4, 2.5 and 2.6 show the probability density of the gain variation for dividers with various dividers and amplifiers. Each curve is obtained as a result of 41 million evaluations of (2.3) and (2.5).

---

<sup>2</sup>AWR Corp. El Segundo, CA 90245, USA, <http://www.awrcorp.com>.

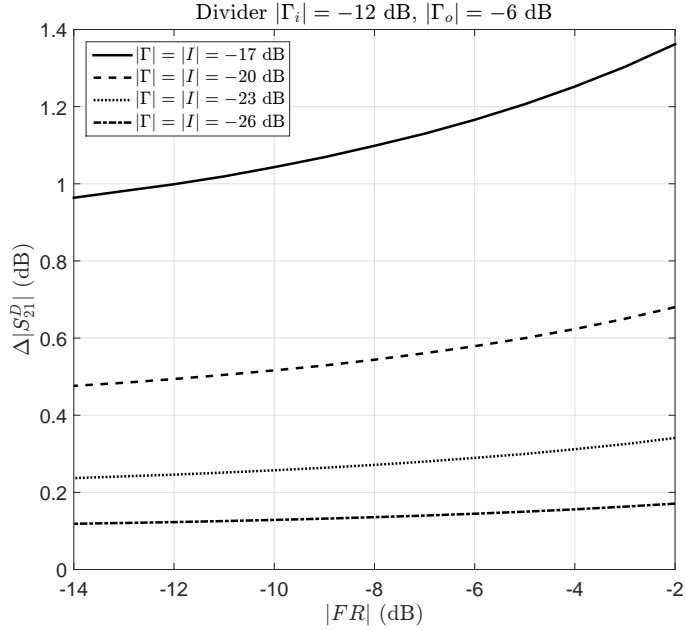


Figure 2.3: The gain variation,  $\Delta|S_{21}^D|$ , for a balanced amplifier with divider for various divider parameters and for amplifiers with  $|\Gamma_i| = -12$  dB,  $|\Gamma_o| = -6$  dB.

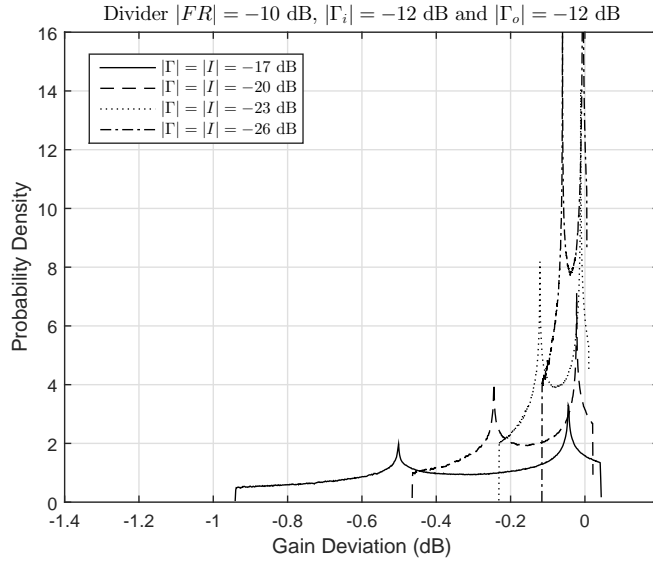


Figure 2.4: The probability density of the gain deviation of a balanced amplifier with divider of various parameters. Amplifiers have  $|FR| = -10$  dB,  $|\Gamma_i| = -12$  dB,  $|\Gamma_o| = -12$  dB.

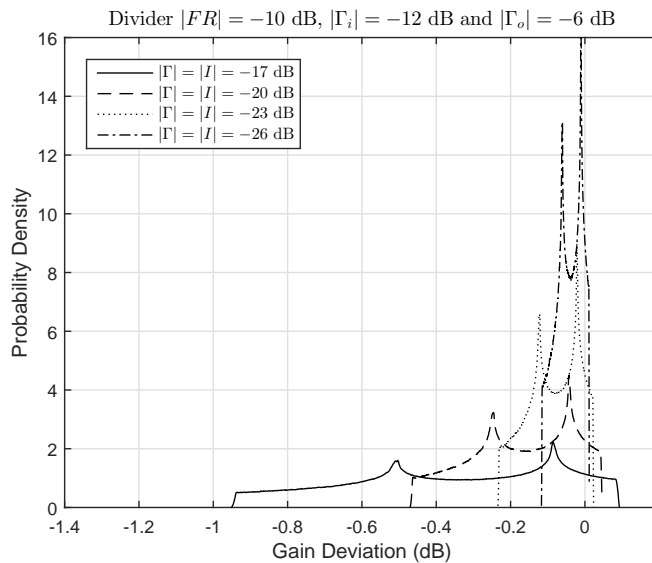


Figure 2.5: The probability density of the gain deviation of a balanced amplifier with divider of various parameters. Amplifiers have  $|FR| = -10$  dB,  $|\Gamma_i| = -12$  dB,  $|\Gamma_o| = -6$  dB.

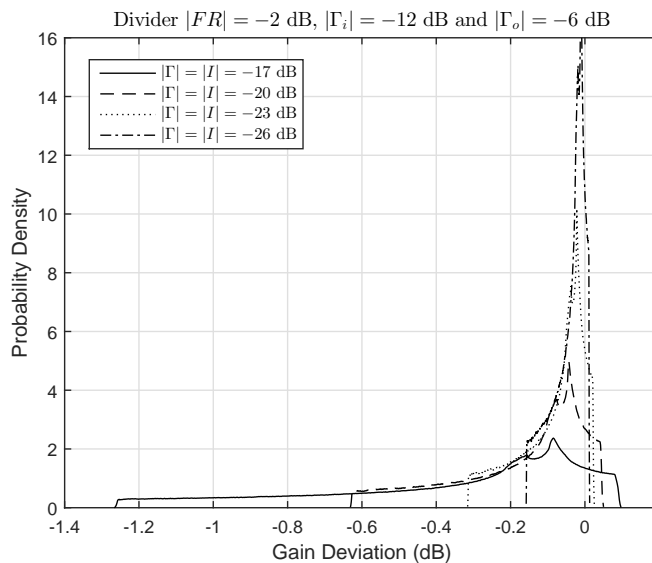


Figure 2.6: The probability density of the gain deviation of a balanced amplifier with divider of various parameters. Amplifiers have  $|FR| = -2$  dB,  $|\Gamma_i| = -12$  dB,  $|\Gamma_o| = -6$  dB.

## 2.2 Balanced Amplifier with 90° Coupler

In Fig. 2.7, a balanced amplifier built with 90° couplers is depicted. The amplifiers and the couplers are assumed to be identical. The S-parameter matrix of the

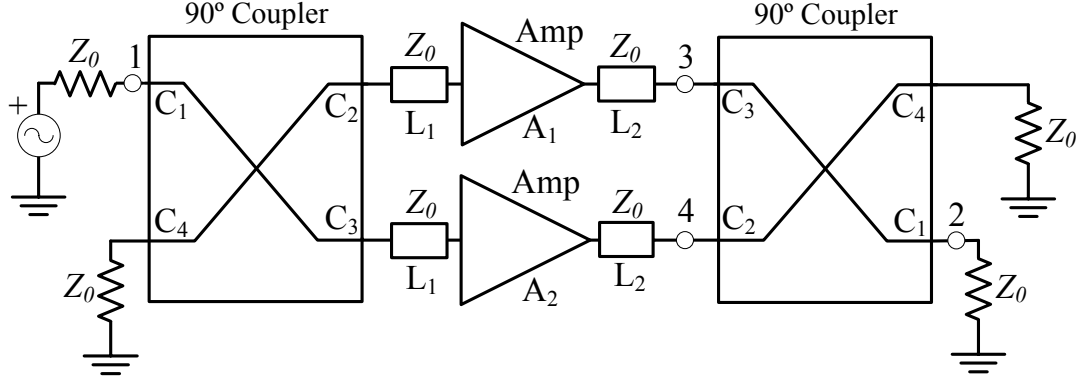


Figure 2.7: A balanced amplifier using 90° couplers.

hybrid coupler,  $S^c$ , with a finite return-loss ( $\Gamma$ ) and isolation ( $I$ ) is given as

$$S^c = \begin{bmatrix} \Gamma & F_d & F_c & I \\ F_d & \Gamma & I & F_c \\ F_c & I & \Gamma & F_d \\ I & F_c & F_d & \Gamma \end{bmatrix}. \quad (2.16)$$

In  $S^c$ ,  $\Gamma$  denotes the return losses of all ports and  $I$  denotes the isolation between the ports  $C_1$ - $C_4$  and  $C_2$ - $C_3$ .  $F_d$  denotes the insertion loss from the ports  $C_1$  to  $C_2$  (also  $C_4$  to  $C_3$ ) whereas  $F_c$  denotes the insertion loss from the ports  $C_1$  to  $C_3$  (also  $C_4$  to  $C_2$ ) of the coupler. Since the hybrid coupler is lossless, we have

$$|\Gamma|^2 + |F_c|^2 + |F_d|^2 + |I|^2 = 1. \quad (2.17)$$

With  $|F_c| = |F_d|$ , we have

$$|F_c| = |F_d| = \frac{\sqrt{1 - |\Gamma|^2 - |I|^2}}{\sqrt{2}}. \quad (2.18)$$

We assume that the phases of  $\Gamma$  and  $I$  are random with uniform distribution. Refer to the flow-graph of the circuit shown in Fig. 2.8. Using, once again,

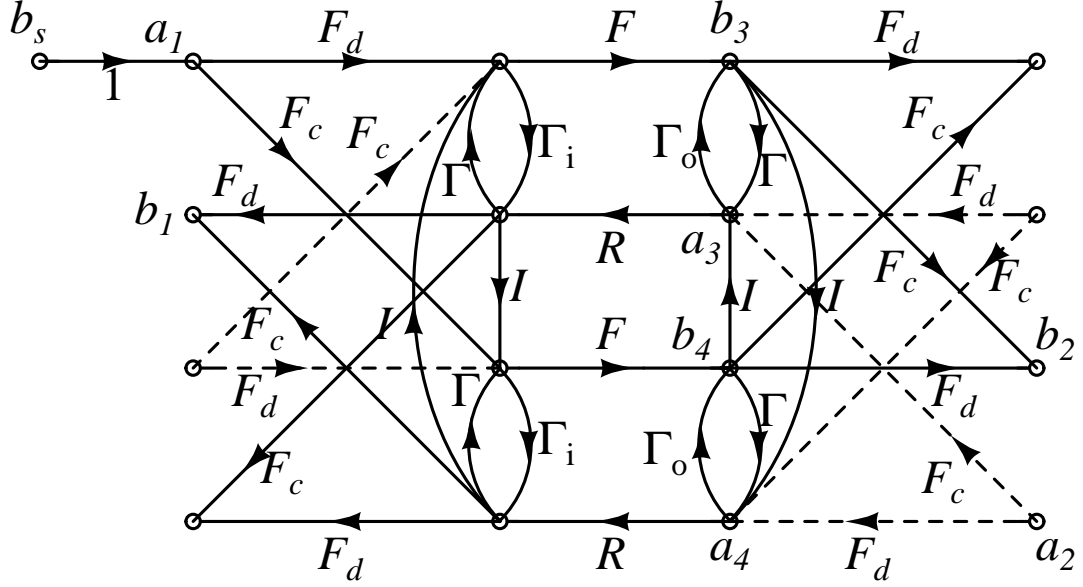


Figure 2.8: Flow graph for the balanced amplifier using coupler. The dashed lines show the irrelevant arms.

Mason's rule<sup>3</sup>, we get the gain as

$$|S_{21}^C| = \left| \frac{b_2}{a_1} \right| = |2FF_cF_d| \left| \frac{\Delta_1}{\Delta_C} \right|, \quad (2.19)$$

where

$$\Delta_1 = 1 - \Gamma(\Gamma_i + \Gamma_o) - (FR - \Gamma_i\Gamma_o)(\Gamma^2 + I^2) \quad (2.20)$$

and

$$\begin{aligned} \Delta_C = & 1 - 2\Gamma(\Gamma_i + \Gamma_o) - 2(FR - \Gamma_i\Gamma_o)(\Gamma^2 + I^2) \\ & + [2\Gamma(\Gamma_i + \Gamma_o)(FR - \Gamma_i\Gamma_o) + (\Gamma_i + \Gamma_o)^2](\Gamma^2 - I^2) \\ & + (FR - \Gamma_i\Gamma_o)^2(\Gamma^2 - I^2)^2. \end{aligned} \quad (2.21)$$

Ignoring the higher order terms,  $\Delta_C$  simplifies to

$$\Delta_C \approx 1 - 2\Gamma(\Gamma_i + \Gamma_o) - 2(FR - \Gamma_i\Gamma_o)(\Gamma^2 + I^2). \quad (2.22)$$

<sup>3</sup>The flow graph has 12 forward paths, 18 loops, 21 non-touching loop pairs, eight non-touching loop triplets and a single non-touching loop quadruplet.

$|S_{21}^C|$  is maximized if  $\Gamma_i$  and  $\Gamma_o$  are of the same phase,  $I^2$  and  $\Gamma^2$  are of the same phase,  $\Gamma(\Gamma_i + \Gamma_o) = |\Gamma(\Gamma_i + \Gamma_o)|$  and  $(FR - \Gamma_i\Gamma_o)(\Gamma^2 + I^2) = |(FR - \Gamma_i\Gamma_o)(\Gamma^2 + I^2)|$  are both positive real. Defining

$$C = |\Gamma(\Gamma_i + \Gamma_o)| + |(FR - \Gamma_i\Gamma_o)(\Gamma^2 + I^2)|, \quad (2.23)$$

the maximum gain,  $|S_{21}^C|_{max}$ , is found as

$$|S_{21}^C|_{max} \approx |2FF_cF_d| \frac{1 - C}{1 - 2C}. \quad (2.24)$$

$|S_{21}^C|$  is minimized if  $\Gamma_i$  and  $\Gamma_o$  are of the same phase,  $I^2$  and  $\Gamma^2$  are of the same phase,  $\Gamma(\Gamma_i + \Gamma_o) = -|\Gamma(\Gamma_i + \Gamma_o)|$  and  $(FR - \Gamma_i\Gamma_o)(\Gamma^2 + I^2) = -|(FR - \Gamma_i\Gamma_o)(\Gamma^2 + I^2)|$  are both negative real. In this case,  $|S_{21}^C|_{min}$  is

$$|S_{21}^C|_{min} \approx |2FF_cF_d| \frac{1 + C}{1 + 2C}. \quad (2.25)$$

Therefore, the gain variation can be found as

$$\Delta|S_{21}^C| \approx \frac{1 + 2C}{1 - 2C} \frac{1 - C}{1 + C} \approx \frac{1 + C}{1 - C}. \quad (2.26)$$

This equation is accurate to within 2%, as long as  $|FR| \leq -2$  dB,  $|\Gamma_i| \leq -8$  dB,  $|\Gamma_o| \leq -8$  dB,  $|\Gamma| \leq -14$  dB and  $|I| \leq -14$  dB. Just like the previous case, decreasing the  $|FR|$  product of the amplifier decreases the gain variation of the balanced amplifier. However, in this case, the input/output return losses of the individual amplifiers have a significant effect on the gain variation. In Fig. 2.9,  $\Delta|S_{21}^C|$  for a balanced amplifier with various coupler and amplifier parameters is given as obtained from the exact equation of (2.19) which is also verified by the linear microwave simulator.

The results of the Monte-Carlo analyses are shown in Figs 2.10, 2.11 and 2.12 as probability density functions of the gain deviation. The amplitudes of the variables are as given, while the phases are random variables with uniform distribution. Each curve is obtained as a result of 41 million evaluations of (2.18) and (2.19).

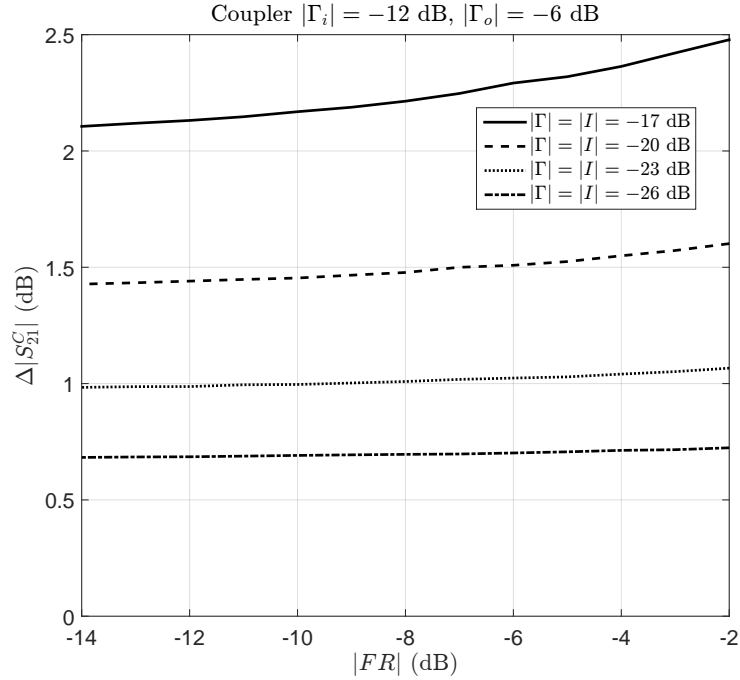


Figure 2.9: The gain variation in  $|S_{21}^C|$  for a balanced amplifier with coupler for various coupler parameters and for amplifiers with  $|\Gamma_i| = -12$  dB and  $|\Gamma_o| = -6$  dB.

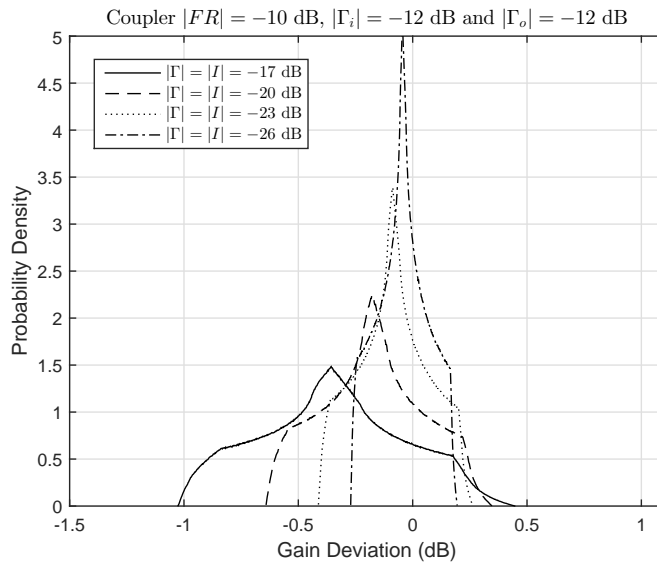


Figure 2.10: The probability density of the gain deviation of a balanced amplifier with coupler of various parameters. Amplifiers have  $|FR| = -10$  dB,  $|\Gamma_i| = -12$  dB,  $|\Gamma_o| = -12$  dB.



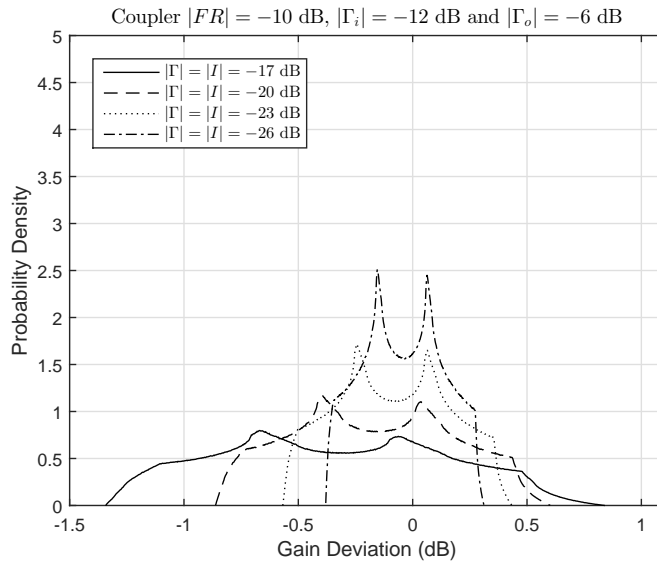


Figure 2.11: The probability density of the gain deviation of a balanced amplifier with coupler of various parameters. Amplifiers have  $|FR| = -10$  dB,  $|\Gamma_i| = -12$  dB,  $|\Gamma_o| = -6$  dB.

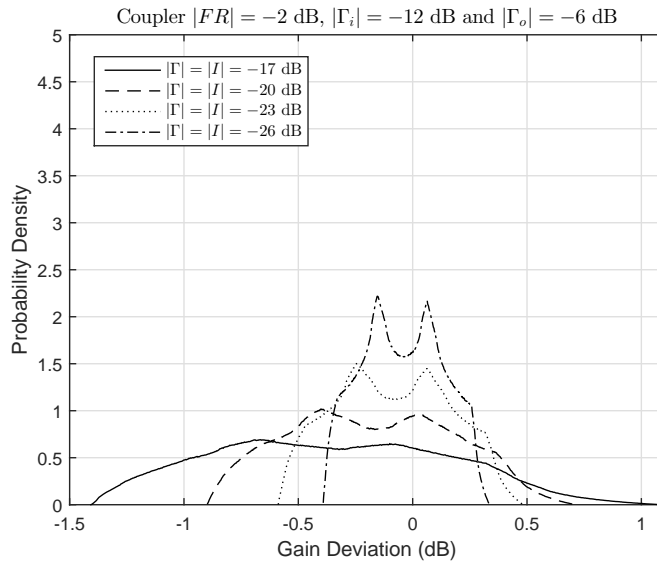


Figure 2.12: The probability density of the gain deviation of a balanced amplifier with coupler of various parameters. Amplifiers have  $|FR| = -2$  dB,  $|\Gamma_i| = -12$  dB,  $|\Gamma_o| = -6$  dB.

## 2.3 Comparison of Gain Variation in Balanced Amplifiers

In the divider case, we can rewrite (2.13) by multiplying both the numerator and the denominator by  $1 - C$  as

$$\Delta|S_{21}^D| \approx \frac{(1 + D - D')(1 - C)}{(1 - D)(1 - C)}. \quad (2.27)$$

Similarly, (2.26) can be written as

$$\Delta|S_{21}^C| \approx \frac{(1 + C)(1 - D)}{(1 - C)(1 - D)}. \quad (2.28)$$

Hence, for  $|\Gamma| \neq 0$  we can state that

$$|\Gamma_i| + |\Gamma_o| > 2|I| - \frac{|FR|}{|\Gamma|} (|\Gamma| - |I|)^2 \Rightarrow \Delta|S_{21}^C| > \Delta|S_{21}^D|. \quad (2.29)$$

This condition on the left is satisfied, for example, if  $|FR| \leq -2$  dB,  $|\Gamma_i| \geq -16$  dB,  $|\Gamma_o| \geq -16$  dB,  $|\Gamma| \leq -17$  dB and  $|I| \leq -17$  dB. Therefore, for most practical cases the gain variation in the balanced amplifier with divider is less than that in the balanced amplifier with coupler.

## 2.4 Experimental Results for Gain Variation

To experimentally verify the gain variation in a balanced amplifier, we consider the divider topology of Fig. 2.1. We chose nearly identical amplifiers ( $A_1$  and  $A_2$ ) that use GALI-84+ from Mini-Circuits<sup>4</sup> at an operating frequency of 1.55 GHz. The measured parameters ( $S^a$  of (2.1)) at 1.55 GHz for amplifiers are given in Table 2.1.

Two identical dividers (with poor return loss and isolation) are manufactured on RO4003<sup>5</sup> 20 mil substrate having 17 dB return loss and 17 dB isolation at 1.55 GHz. Table 2.2 lists the entries of  $S^d$  given in (2.1). By using these

<sup>4</sup>Mini-Circuits, NY 11235, USA, <http://www.minicircuits.com>

<sup>5</sup>Rogers Corp. Rogers, CT 06263, USA, <http://www.rogerscorp.com>

		$\Gamma_i$	$F$	$R$	$\Gamma_o$
$A_1$	dB	-14.6	21.4	-28	-8.9
	Angle	109°	-17.5°	-107.5°	27.4°
$A_2$	dB	-13.7	21.2	-28	-9.6
	Angle	109.3°	-21.3°	-110°	22.4°

Table 2.1: S-Parameters in dB magnitude-angle format measured at 1.55 GHz for amplifiers

		$\Gamma_c$	$F_c$	$\Gamma$ (port 2, 3)	$I$
$D_{11}$	dB	-10.7	-3.55	-17.2, -16.9	-16.8
	Angle	120°	-116.0°	89.3°, 86.7°	129.7°
$D_{12}$	dB	-10.9	-3.56	-17.3, -17.1	-17.0
	Angle	118.2°	-115.8°	90.7°, 91.6°	130.4°

Table 2.2: S-parameters measured for both dividers at 1.55 GHz in dB magnitude-angle format.

amplifiers and dividers (Fig. 2.13), the gain variation of the balanced amplifier is measured. Identical SMA line extenders (also shown in Fig. 2.13) each with the loss of 0.01 dB and phase shift of 35° at 1.55 GHz are used to vary the transmission-line length between the amplifiers and the dividers. Fig. 2.14 shows the theoretical and the measured gain reduction from the maximum in balanced amplifier. The theoretical values are obtained from the exact expression of (2.5) with varying the length of  $L_1$  which is added to the parameters  $F$ ,  $R$  and  $\Gamma_i$  as a phase shift. The measured gain variation is consistent with the theoretical calculations that can be observed from Fig. 2.14.

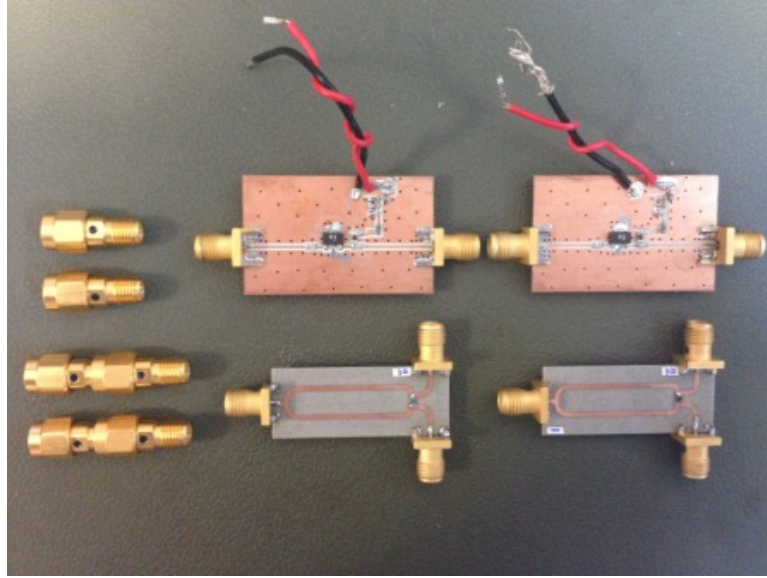


Figure 2.13: The photo of the dividers, amplifiers and some of the SMA line extenders used for balanced amplifier's gain and power reduction measurements.

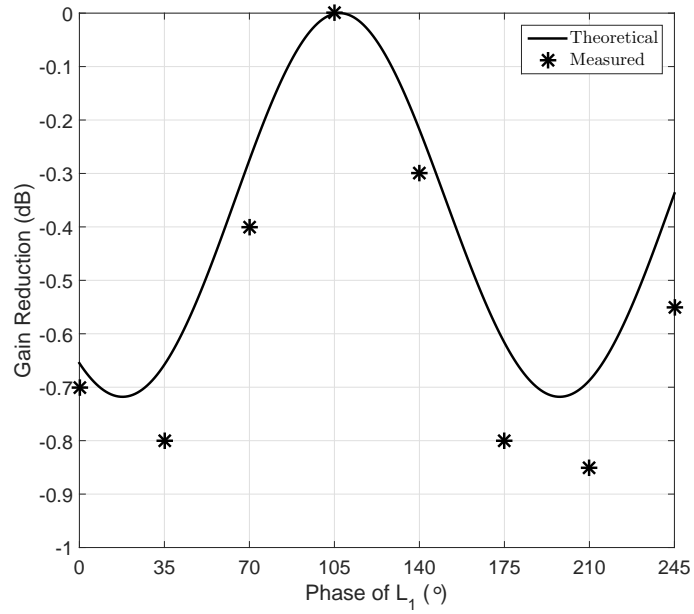


Figure 2.14: The theoretical and measured gain reduction in balanced amplifier versus transmission-line length between the amplifiers and the dividers. The measured gain variation is consistent with the theoretical calculations.

# Chapter 3

## Noise Figure Analysis of a Balanced Amplifier

### 3.1 Noise Waves for the Balanced Amplifier

The noise figure of a stand-alone amplifier,  $F$ , can be written in terms of its source impedance,  $\Gamma_s$ , as [41]

$$F = F_m + 4r_n \frac{|\Gamma_s - \Gamma_o|^2}{(1 - |\Gamma_s|^2)|1 + \Gamma_o|^2}, \quad (3.1)$$

where  $r_n$  is the normalized equivalent noise resistance,  $\Gamma_o$  is the optimal source reflection coefficient to obtain the minimum noise figure,  $F_m$ . Suppose that we use two such amplifiers with  $\Gamma_o=0$  and two identical 2-way  $0^\circ$  power dividers/combiners to build a balanced amplifier as depicted in Fig. 3.1. Fig. 3.1 is a modified version of Fig. 2.1, where the interconnections are included in the amplifier parameters and the source has an impedance of  $Z_s$  ( $\Gamma_s$ ). S-parameters of the amplifiers ( $S^a$ ) and the dividers ( $S^d$ ) all specified with respect to  $Z_0$  are also shown in matrix form. Some of the notations in the matrices are intentionally chosen different from the representation in Chapter 2 to avoid confusions for the analysis given here. In  $S^d$  matrix,  $\Gamma_r$ ,  $\Gamma_1$  and  $\Gamma_2$  are the return loss of the divider ports 1, 2 and 3 respectively.  $I$  denotes the isolation between the ports

2 and 3.  $A_{r1}$  is the insertion loss between the ports 1 and 2 whereas  $A_{r2}$  is the insertion loss between the ports 1 and 3. In  $S^a$ ,  $\Gamma_i$  is the input return loss and  $A$  is the gain of the amplifier.

The noise wave representation is an important approach to determine the noise figure of a linear noisy device [41–48]. To find an analytical expression for the noise figure of the balanced amplifier, we use the noise wave approach [41]. The noise waves and the correlation matrix for the divider can be found from the real part of its Y-parameters [47], while the noise waves for the amplifiers can be written in terms of their noise parameters [43].

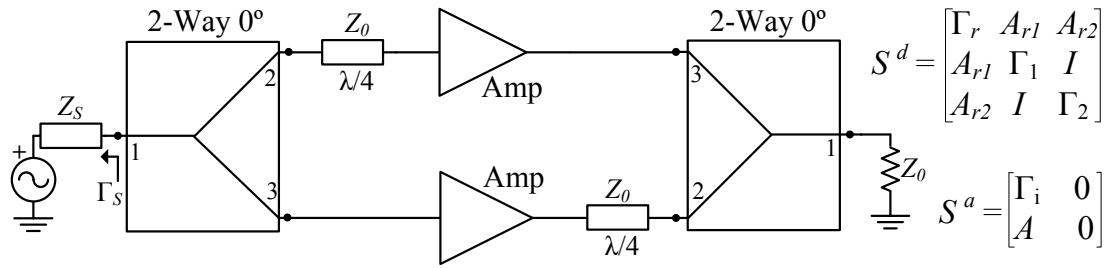


Figure 3.1: A balanced amplifier built using 2-way  $0^\circ$  power dividers.

### 3.1.1 Noise Waves for the Amplifiers

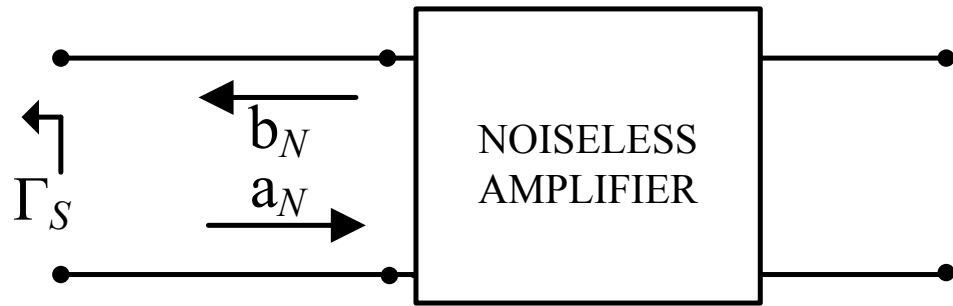


Figure 3.2: The representation of a noisy amplifier by noise waves.

First, we will find the additional noise generated by the amplifiers. A noisy amplifier can be represented by a noiseless two-port amplifier and two uncorrelated noise waves existing at the input of the amplifier [41, 42] as shown in Fig. 3.2. The flow graph in Fig. 3.3 can be used to find the noise figure of the balanced amplifier,  $F_d$ , with ideal lossless dividers. Here,  $a_{n1}$ ,  $b_{n1}$  are two uncorrelated noise waves at the input of the upper amplifier whereas  $a_{n2}$ ,  $b_{n2}$  are of the lower amplifier. So, the output noise powers generated by these two uncorrelated sources for each amplifier are

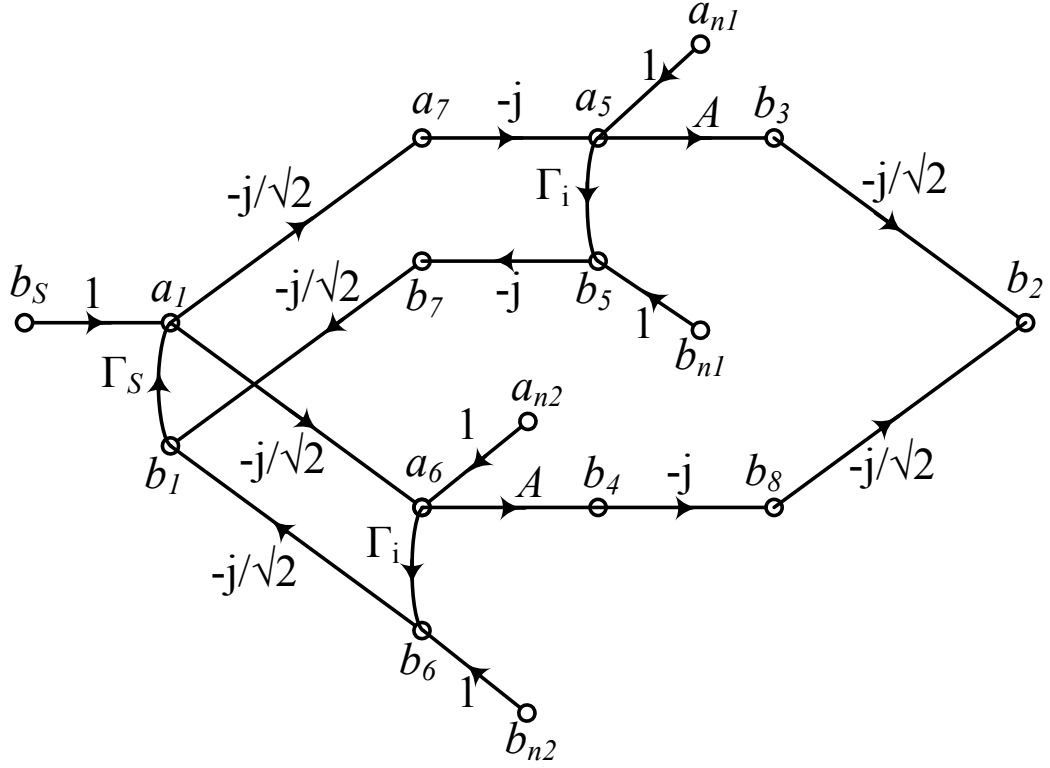


Figure 3.3: The flow graph of the balanced amplifier built using lossless ideal power dividers.

$$N_{a1} = \left| \frac{b_2}{a_5} \right|^2 (F_m - 1) + \left| \frac{b_2}{b_5} \right|^2 (4r_n - F_m + 1), \quad (3.2)$$

$$N_{a2} = \left| \frac{b_2}{a_6} \right|^2 (F_m - 1) + \left| \frac{b_2}{b_6} \right|^2 (4r_n - F_m + 1). \quad (3.3)$$

We can apply the Mason's rule to find the transfer functions as,

$$\frac{b_2}{a_5} = -j \frac{A}{\sqrt{2}} (1 + \Gamma_s \Gamma_i), \quad \frac{b_2}{b_5} = -j \frac{A}{\sqrt{2}} \Gamma_s \quad (3.4)$$

and

$$\frac{b_2}{a_6} = -\frac{A}{\sqrt{2}} (1 - \Gamma_s \Gamma_i), \quad \frac{b_2}{b_6} = \frac{A}{\sqrt{2}} \Gamma_s. \quad (3.5)$$

Finally, the output noise powers,  $N_{a1}$  and  $N_{a2}$ , generated by each amplifier are

$$N_{a1} = \frac{|A|^2}{2} |1 + \Gamma_s \Gamma_i|^2 (F_m - 1) + \frac{|A|^2}{2} |\Gamma_s|^2 (4r_n - F_m + 1), \quad (3.6)$$

$$N_{a2} = \frac{|A|^2}{2} |1 - \Gamma_s \Gamma_i|^2 (F_m - 1) + \frac{|A|^2}{2} |\Gamma_s|^2 (4r_n - F_m + 1). \quad (3.7)$$

### 3.1.2 Noise Waves for the Input and Output Dividers

Then, the additionally generated noise powers by the input and output dividers should be found. A noisy three-port divider can be represented by a noiseless three-port admittance network and three noise current sources  $i_{n1}$ ,  $i_{n2}$  and  $i_{n3}$  as shown in Fig. 3.4. To find the output noise power of a passive network, these current noise sources can be used and the overall power can be determined by calculating the noise power due to each current source.

The output noise power generated by a three-port divider is

$$\begin{aligned} N_r = & |T_1|^2 |i_{n1}|^2 + |T_2|^2 |i_{n2}|^2 + |T_3|^2 |i_{n3}|^2 + \\ & T_1 T_2^* i_{n1} i_{n2}^* + T_1^* T_2 i_{n1}^* i_{n2} + T_1 T_3^* i_{n1} i_{n3}^* + T_1^* T_3 i_{n1}^* i_{n3} + \\ & T_2 T_3^* i_{n2} i_{n3}^* + T_2^* T_3 i_{n2}^* i_{n3}, \end{aligned} \quad (3.8)$$

where  $T$  is the transfer function from the related noise source to the output. Here,  $*$  denotes the conjugate operator.

The correlation matrix for a passive 3-port device can be written in terms of the noise current sources as

$$C^d = \begin{bmatrix} |i_{n1}|^2 & i_{n1} i_{n2}^* & i_{n1} i_{n3}^* \\ i_{n2} i_{n1}^* & |i_{n2}|^2 & i_{n2} i_{n3}^* \\ i_{n3} i_{n1}^* & i_{n3} i_{n2}^* & |i_{n3}|^2 \end{bmatrix}. \quad (3.9)$$



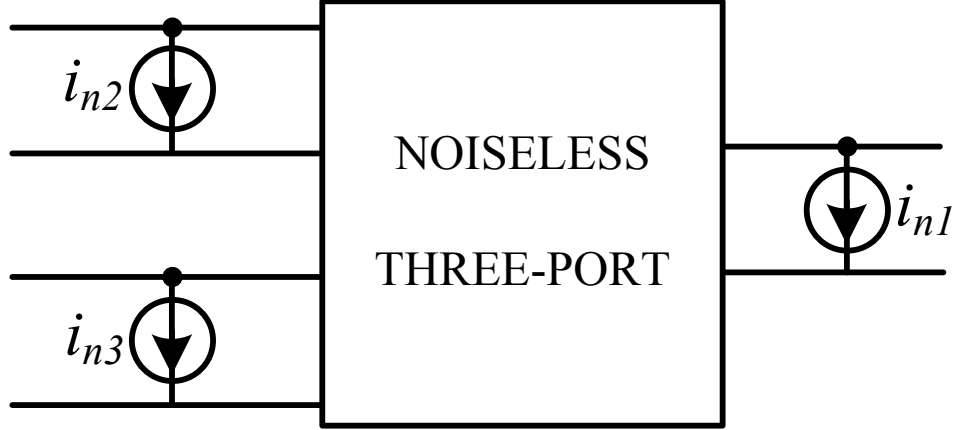


Figure 3.4: The representation of a noisy three-port network by current sources.

Besides,

$$C^d = 2kT_0 \text{Re}\{Y^d\}. \quad (3.10)$$

The Y-parameter matrix of the lossless ideal divider is

$$Y^d = Y_0 \begin{bmatrix} 0 & \frac{j}{\sqrt{2}} & \frac{j}{\sqrt{2}} \\ \frac{j}{\sqrt{2}} & \frac{1}{2} & -\frac{1}{2} \\ \frac{j}{\sqrt{2}} & -\frac{1}{2} & \frac{1}{2} \end{bmatrix}. \quad (3.11)$$

The correlation matrix of the divider simplifies to

$$C^d = 2kT_0 Y_0 \begin{bmatrix} 0 & 0 & 0 \\ 0 & \frac{1}{2} & -\frac{1}{2} \\ 0 & -\frac{1}{2} & \frac{1}{2} \end{bmatrix}, \quad (3.12)$$

where  $2kT_0 Y_0$  can be normalized to 1 for simplicity.

By the help of (3.8), output noise power for the input divider,  $N_{r1}$ , is

$$N_{r1} = \left| \frac{b_2}{a_7} \right|^2 |i_{n2}|^2 + \left| \frac{b_2}{a_6} \right|^2 |i_{n3}|^2 + \left( \frac{b_2}{a_7} \right) \left( \frac{b_2}{a_6} \right)^* i_{n2} i_{n3}^* + \left( \frac{b_2}{a_7} \right)^* \left( \frac{b_2}{a_6} \right) i_{n2}^* i_{n3}. \quad (3.13)$$

In the same manner, output noise power resulting from output divider,  $N_{r2}$ , is

$$N_{r2} = \left| \frac{b_2}{b_3} \right|^2 |i_{n2}|^2 + \left| \frac{b_2}{b_8} \right|^2 |i_{n3}|^2 + \left( \frac{b_2}{b_3} \right) \left( \frac{b_2}{b_8} \right)^* i_{n2} i_{n3}^* + \left( \frac{b_2}{b_3} \right)^* \left( \frac{b_2}{b_8} \right) i_{n2}^* i_{n3}. \quad (3.14)$$

The transfer functions for the input and the output dividers should be found separately. For the input divider, applying the Mason's rule,

$$\frac{b_2}{a_7} = -\frac{A}{\sqrt{2}}(1 + \Gamma_s \Gamma_i), \quad \frac{b_2}{a_6} = -\frac{A}{\sqrt{2}}(1 - \Gamma_s \Gamma_i). \quad (3.15)$$

For the output divider,

$$\frac{b_2}{b_3} = \frac{b_2}{b_8} = -\frac{j}{\sqrt{2}}. \quad (3.16)$$

Finally, the output noise powers generated by the dividers can be obtained as

$$N_{r1} = |A|^2 |\Gamma_s \Gamma_i|^2, \quad N_{r2} = 0. \quad (3.17)$$

### 3.1.3 Noise Waves for the Input Source

Lastly, the output noise power due to the input source,  $N_s$ , is

$$N_s = \left| \frac{b_2}{b_s} \right|^2 (1 - |\Gamma_s|^2) = \left| \frac{b_2}{a_1} \right|^2 (1 - |\Gamma_s|^2). \quad (3.18)$$

Here, the overall transfer function,  $\left| \frac{b_2}{a_1} \right|$ , can be found by using (2.5) as,

$$\left| \frac{b_2}{a_1} \right| = \left| 2A \left( \frac{-j}{\sqrt{2}} \right)^2 \right|. \quad (3.19)$$

Finally,

$$\left| \frac{b_2}{a_1} \right| = |A|. \quad (3.20)$$

## 3.2 Noise Figure of a Balanced Amplifier

### 3.2.1 Noise Figure of a Balanced Amplifier

The noise figure,  $F_d$ , of the 2-port balanced amplifier can be expressed as

$$F_d = 1 + \frac{N_{r1} + N_{r2} + N_{a1} + N_{a2}}{N_s}. \quad (3.21)$$

By using the noise wave approach, the noise powers are found to determine the  $F_d$ . The parameters in  $S_d$  include the imperfections of the divider, such as finite ohmic loss, return loss and isolation. If needed, any imperfection of the  $\lambda/4$  line can also be represented by  $S_d$ . We assume that the gain of the amplifiers is sufficiently high and the output combiner is perfectly balanced so that the output combiner does not influence the noise figure.

**Corollary 1** *If  $\beta$  is a complex number, then*

$$|1 + \beta|^2 + |1 - \beta|^2 = 2(1 + |\beta|^2). \quad (3.22)$$

Proof: Denoting  $\beta = |\beta|e^{j\phi}$ ,

$$\begin{aligned} |1 + \beta|^2 + |1 - \beta|^2 &= |1 + |\beta|e^{j\phi}|^2 + |1 - |\beta|e^{j\phi}|^2 \\ &= 1 + |\beta|^2 + 2|\beta|\cos\phi + 1 + |\beta|^2 - 2|\beta|\cos\phi \\ &= 2(1 + |\beta|^2). \end{aligned}$$

Using (3.21), (3.6), (3.7), (3.17) and (3.22), the noise figure of the balanced amplifier with ideal dividers is

$$F_d = 1 + \frac{|A|^2(1 + |\Gamma_s\Gamma_i|^2)(F_m - 1) + |A|^2|\Gamma_s|^2(4r_n - F_m + 1) + |A|^2|\Gamma_s\Gamma_i|^2}{|A|^2(1 - |\Gamma_s|^2)}. \quad (3.23)$$

With further simplification,

$$F_d = 1 + \frac{F_m(1 - |\Gamma_s|^2) - (1 - |\Gamma_s|^2) + F_m|\Gamma_s\Gamma_i|^2 + 4r_n|\Gamma_s|^2}{1 - |\Gamma_s|^2}. \quad (3.24)$$

And finally, the noise figure of the balanced amplifier with an ideal lossless input divider can be written as

$$F_d = F_m + 4 \left( r_n + F_m \frac{|\Gamma_i|^2}{4} \right) \frac{|\Gamma_s|^2}{1 - |\Gamma_s|^2}. \quad (3.25)$$

With a non-zero  $|\Gamma_i|$ , the input divider is terminated with different impedances at its output ports, and thus the isolation resistor of the divider contributes to the output noise. When  $\Gamma_i = 0$ , the symmetry is satisfied and the noise figure of the balanced amplifier is the same as that of the single amplifier. Note that the noise figure is independent of the phases of  $\Gamma_i$  and  $\Gamma_s$ . The normalized equivalent noise resistance is increased to  $r_n + F_m|\Gamma_i|^2/4$ , while  $F_m$  and  $\Gamma_o = 0$  remain unchanged.

Fig. 3.5 have plots of noise figure variation as a function of  $|\Gamma_s|$  for amplifiers with  $F_m=1$  dB. The noise figure of a balanced amplifier is degraded in comparison to a single amplifier for the same source return loss. The noise figure of a single amplifier does not depend on the amplifier's input impedance whereas the balanced amplifier's noise figure is dependent on it. Fig. 3.6 shows the noise figure degradation as a function of  $F_m$  for various  $r_n$  values. The parameters are kept constant where  $|\Gamma_i|=-7$  dB,  $|\Gamma_s|=-10$  dB. For the increasing  $F_m$ , the degradation decreases where the dominance of  $|\Gamma_i|$  starts to get less.

The exact noise figure expression is determined using a symbolic computational package<sup>1</sup>. The resulting expressions are verified numerically by two separate linear microwave simulators.<sup>2</sup>

Using the exact noise figure expression, Fig. 3.7 presents the maximum value of  $|\Gamma_r|$  to limit the noise figure degradation for  $\Gamma_s = 0$  to 0.1 dB for the lossless and balanced divider with  $\Gamma = \Gamma_1 = \Gamma_2$ . For example, consider a balanced amplifier built from two amplifiers with  $F_m=0.4$  dB,  $r_n=0.6$  and  $\Gamma_o=0$ . We need to use a lossless divider with  $\{|\Gamma_r|, |\Gamma|, |I|\} \leq -21$  dB, to get a noise figure less than 0.5 dB. If the input divider is not perfect, there may be further degradation. The full noise figure expression is too long to be given here. Assuming  $\Gamma = \Gamma_1 = \Gamma_2$ , it can be written approximately as

$$F_d \approx \frac{\frac{F_m}{2}(|\rho_a|^2 + |\rho_b|^2) + 4(r_n - \frac{F_m}{4})|\rho_c|^2}{\frac{|\rho_d|^2}{2}(1 - |\Gamma_s|^2)}, \quad (3.26)$$

<sup>1</sup>Symbolic toolbox of MATLAB, Mathworks, <https://www.mathworks.com/>

<sup>2</sup>AWR from AWR Corp. (<http://www.awrcorp.com>) and ADS from Keysight Technologies ([www.keysight.com](http://www.keysight.com)).

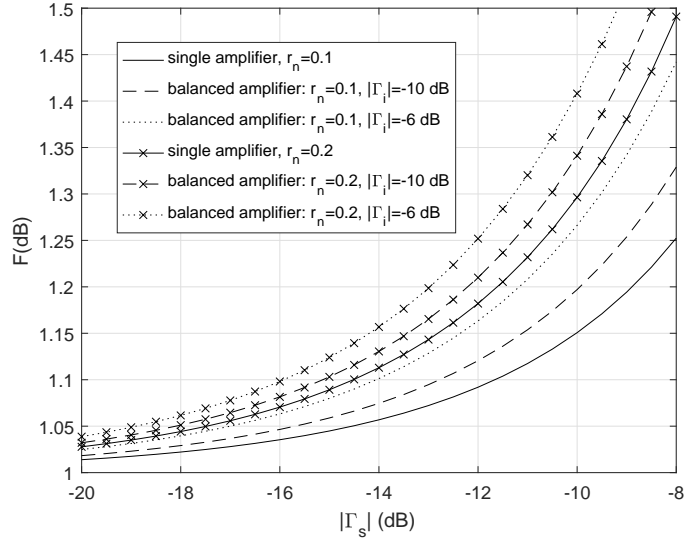


Figure 3.5: The noise figures of single and balanced amplifiers with perfect dividers as a function of source reflection coefficient. Amplifiers have  $F_m=1$  dB,  $\Gamma_o=0$  and various  $r_n$  and  $|\Gamma_i|$  values. The noise figure of a balanced amplifier is degraded in comparison to a single amplifier for the same source return loss.

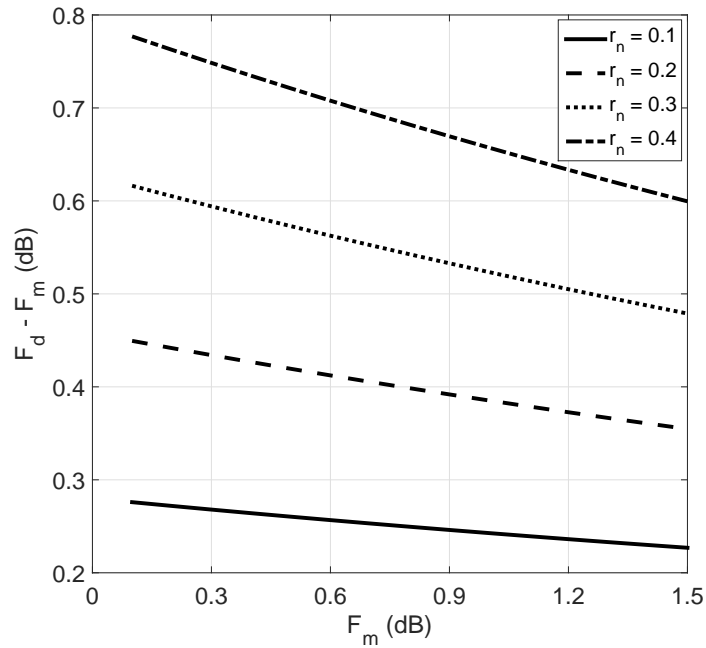


Figure 3.6: The noise figure degradation of balanced amplifiers with perfect dividers as a function of  $F_m$ . Amplifiers have  $|\Gamma_i|=-7$  dB,  $|\Gamma_s|=-10$  dB,  $\Gamma_o=0$  and various  $r_n$  values.

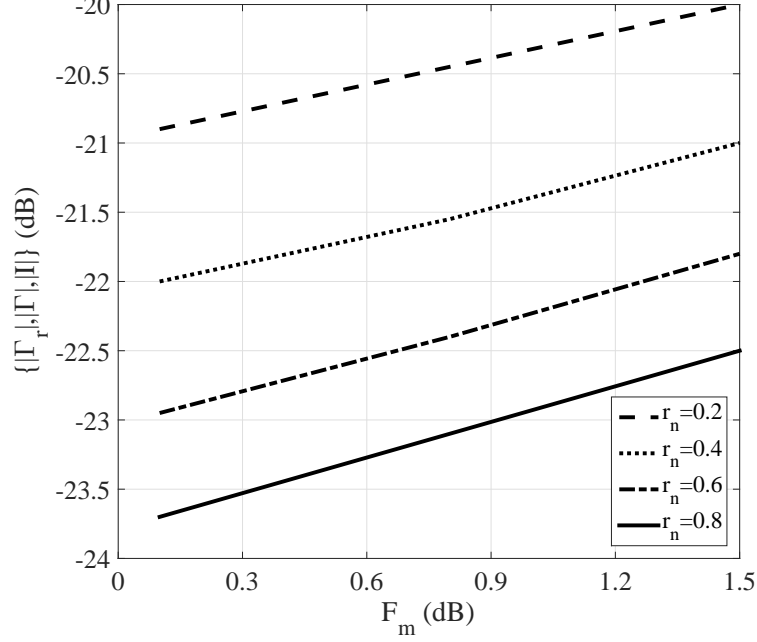


Figure 3.7: The maximum value of the divider  $|\Gamma_r|$  to limit the noise figure degradation in the balanced amplifier with 2-way dividers to 0.1 dB for  $\Gamma_s=0$ . The amplifiers have  $|\Gamma_i|=-7$  dB

where

$$\begin{aligned}
\rho_a &= \Gamma_i(\Gamma_s[A_{r1}^2 + A_{r1}A_{r2}] + \Gamma + I) - (\Gamma_r\Gamma_s - 1), \\
\rho_b &= \Gamma_i(\Gamma_s[A_{r2}^2 + A_{r1}A_{r2}] + \Gamma + I) + (\Gamma_r\Gamma_s - 1), \\
\rho_c &= \Gamma + I + \Gamma_s \frac{(A_{r1} + A_{r2})^2}{2}, \\
\rho_d &= A_{r1} + A_{r2} + (A_{r2} - A_{r1})\Gamma_i(\Gamma + I).
\end{aligned}$$

If we consider a perfectly symmetric but lossy divider, then 3.26 will simplify to

$$\begin{aligned}
F_d &\approx \frac{F_m}{\alpha} + \frac{4(r_n + F_m \frac{|\Gamma_i|^2}{4})|\Gamma_x|^2}{\alpha(1 - |\Gamma_r|^2)(1 - |\Gamma_s|^2)} \\
&\quad + \frac{F_m(|\Gamma_s|^2 - 1 - |\Gamma_x|^2 + |1 - \Gamma_r\Gamma_s|^2 + (1 - |\Gamma_s|^2)|\Gamma_r|^2)}{\alpha(1 - |\Gamma_r|^2)(1 - |\Gamma_s|^2)} \\
&\quad \text{with } \Gamma_x = \Gamma + I + 2A_r^2\Gamma_s \quad \text{and} \quad \alpha \triangleq \frac{2|A_r|^2}{1 - |\Gamma_r|^2}. \quad (3.27)
\end{aligned}$$

Here,  $\alpha$  defines the ohmic loss of the divider and we have  $\Gamma = \Gamma_1 = \Gamma_2$  and  $A_r = A_{r1} = A_{r2}$ . The approximation in (3.27) is accurate to within  $\pm 0.03$  dB, for  $\{|\Gamma_r|, |\Gamma|, |I|\} \leq -17$  dB,  $|\Gamma_i| \leq -7$  dB,  $\alpha > -1$  dB and  $|\Gamma_s| \leq -10$  dB. Note that for  $\Gamma_r = \Gamma = I = 0$  and  $\alpha = 1$ , (3.27) reduces to (3.25).

We ignore the last term of  $F_d$  expression in (3.27) and since  $|A_r|^2(\Gamma + I) \approx -A_r^2\Gamma_r^*$  we let  $|\Gamma_x| \approx |\Gamma_s - \Gamma_r^*|$ , to find the approximate noise parameters of the balanced amplifier  $F_{md}$ ,  $\Gamma_{od}$  and  $r_{nd}$  as

$$F_{md} \approx \frac{F_m}{\alpha}, \quad \Gamma_{od} \approx \Gamma_r^*, \quad r_{nd} \approx \left( r_n + F_m \frac{|\Gamma_i|^2}{4} \right) \frac{|1 + \Gamma_r|^2}{\alpha(1 - |\Gamma_r|^2)}, \quad (3.28)$$

where  $*$  is the conjugate operator. We observe that  $F_{md}$  increases,  $r_{nd}$  may increase or decrease and  $\Gamma_{od}$  is no longer zero. Note that the noise parameters depend on  $\alpha$  and  $\Gamma_r$ , but not on  $\Gamma$  or  $I$ . In (3.28), the accuracy of the parameters is given by:  $F_{md}$ :  $\pm 0.005$  dB,  $r_{nd}$ :  $\pm 8\%$ ,  $|\Gamma_{od}|$ :  $\pm 0.02$ , as long as  $\{|\Gamma_r|, |\Gamma|, |I|\} \leq -17$  dB,  $\alpha > -0.2$  dB and  $r_n > 0.1$ . The noise parameters can be calculated using (3.1) for different source impedances as described in [49] or using correlation matrix method as described in [48] but (3.28) offers a very good approximation for these parameters.

Fig. 3.8 presents calculated the noise figure of the balanced amplifier under different conditions. The curves are obtained using the exact noise figure expressions in a Monte Carlo simulation. Wilkinson dividers are built with two lossy transmission lines and an isolation impedance, the parameters of which have a statistical distribution. 50,000 dividers with return loss and isolation better than 20, 26 or 32 dB and with an ohmic loss of 0.1 dB are considered. The phases of the source impedance and amplifier parameters are also chosen randomly for each simulation. The graphs show the worst case values of the noise figure. The noise figure of the stand-alone amplifier is also given for comparison.

Fig. 3.9 shows the calculated noise figure degradation of the balanced amplifier which are obtained using the exact noise figure expressions in a Monte Carlo simulation under different return loss and isolation values of the divider.  $|\Gamma_s|$  is kept constant to  $-10$  dB and the degradation is presented for various  $r_n$  values of the amplifier. Fig. 3.9 states the importance of the return loss and isolation

values of the divider. As  $\{|\Gamma_r|, |\Gamma|, |I|\}$  get higher values in dB, the degradation in the noise figure becomes more.

Using the curves in Fig. 3.8 we can investigate the possible benefit of a ferrite isolator in the noise figure when the source has a low return loss (e.g., an antenna). For example, suppose that the source has  $|\Gamma_s| = -9.5$  dB. If an isolator with an insertion loss of 0.10 dB giving a return loss of 20 dB is inserted at the input of the single amplifier, the noise figure improves from 1.17 dB to  $1.02 + 0.10 = 1.12$  dB. If we place the same isolator at the input of the balanced amplifier with 20 dB divider, we get  $1.20 + 0.10 = 1.30$  dB instead of 1.58 dB.

### 3.2.2 Amplitude and Phase Imbalance

To determine the effect of phase and amplitude imbalance of the input and output dividers on the noise figure, the full noise figure expression should be used and processed. For unideal input and output dividers, the full long noise figure expression simplifies as

$$F_d \approx \frac{F_m \left( \frac{|\Gamma_s \Gamma_i \rho_x + 1|^2}{4|A_{r2}|^2} + \frac{|\Gamma_s \Gamma_i \rho_x - 1|^2}{4|A_{r1}|^2} \right) + 4 \left( r_n + F_m \frac{|\Gamma_i|^2}{4} \right) |\Gamma_s|^2 \rho_x}{1 - |\Gamma_s|^2}, \quad (3.29)$$

where

$$\rho_x = (A_{r1}^2 + A_{r2}^2). \quad (3.30)$$

Note that any attenuation or phase error in the  $\lambda/4$  transmission lines also generate these errors. We found that an amplitude or phase imbalance may result in a noise figure degradation or improvement depending on the phases of  $\Gamma_s$  and  $\Gamma_i$ . Assume that, the input divider is lossless and there is an amplitude imbalance in between each arms of the divider defined by  $A_{r1}/A_{r2} = 1 + 2x$  where  $x$  is small. Then, using 3.26, for an amplitude imbalance less than 0.4 dB, the noise figure of the balanced amplifier as a function of the amplitude imbalance can be obtained as

$$F_d \approx F_m + 4 \left( r_n + F_m \frac{|\Gamma_i|^2}{4} \pm \frac{F_m}{2} \left| \frac{\Gamma_i}{\Gamma_s} \right| x \right) \frac{|\Gamma_s|^2}{1 - |\Gamma_s|^2}. \quad (3.31)$$



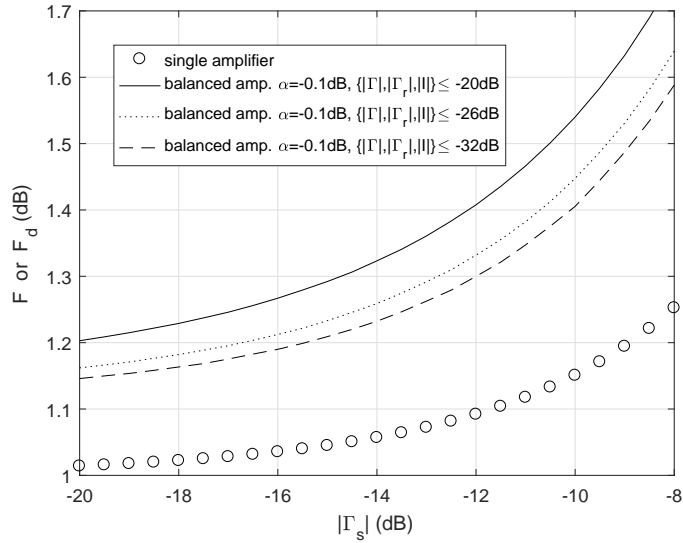


Figure 3.8: The worst-case noise figure as a function of source reflection coefficient for a balanced amplifier. The input divider has an ohmic loss of 0.1 dB, and return loss and isolation better than 20 dB, 26 dB or 32 dB. The amplifiers have  $|\Gamma_i| = -7$  dB,  $F_m = 1$  dB,  $r_n = 0.1$  and  $\Gamma_o = 0$ .

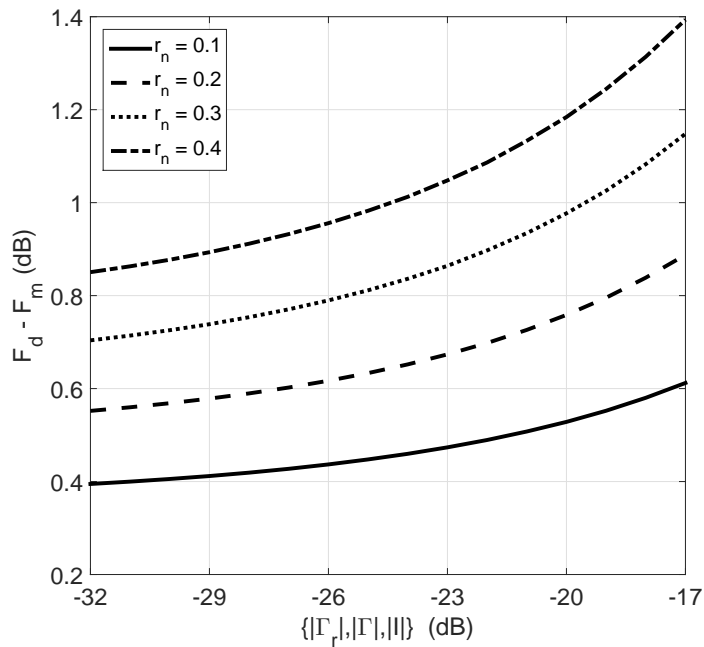


Figure 3.9: The noise figure degradation as a function of the return loss and isolation for a balanced amplifier. The input divider has an ohmic loss of 0.1 dB, and  $|\Gamma_s| = -10$  dB. The amplifiers have  $|\Gamma_i| = -7$  dB,  $F_m = 1$  dB,  $\Gamma_o = 0$  and various  $r_n$  values.

For the same amplitude imbalance on the output divider, with the help of 3.29, the noise figure now lies in the range

$$F_d \approx F_m + 4 \left( r_n + F_m \frac{|\Gamma_i|^2}{4} \pm F_m \left| \frac{\Gamma_i}{\Gamma_s} \right| x \right) \frac{|\Gamma_s|^2}{1 - |\Gamma_s|^2}. \quad (3.32)$$

For example, with  $F_m=1$  dB,  $r_n = 0.1$ ,  $|\Gamma_i| = -7$  dB,  $|\Gamma_s| = -10$  dB, lossless dividers with 0.2 dB imbalance may result in at most 0.03 dB noise figure degradation or improvement. Fig. 3.10 is given to show the effect of the amplitude imbalance on the noise figure for different  $\Gamma_s$  values. The ohmic loss is also added to each arm of the divider. The amplitude imbalance may improve or degrade the noise figure but this influence is small if the imbalance is less than 0.5 dB. Besides, the noise figure increases at least as the amount of the loss emphasizing the importance of the ohmic loss on the noise figure.

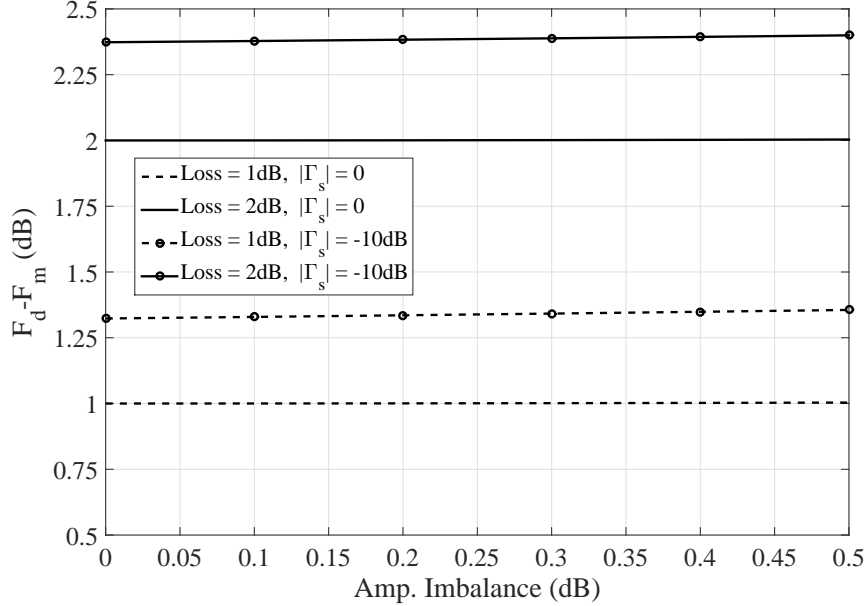


Figure 3.10: Noise figure degradation with respect to the amplitude imbalance. The amplifiers have  $|\Gamma_i|=-7$  dB,  $F_m=1$  dB,  $r_n = 0.1$  and  $\Gamma_o=0$ .

If only the input divider has a phase error defined by  $A_{r1}/A_{r2} = e^{j\theta}$ , for a phase imbalance less than  $10^\circ$ , the noise figure is in the range

$$F_d \approx F_m + 4 \left( r_n + F_m \frac{|\Gamma_i|^2}{4} \pm F_m \left| \frac{\Gamma_i}{\Gamma_s} \right| \frac{\theta}{4} \right) \frac{|\Gamma_s|^2}{1 - |\Gamma_s|^2} \quad (3.33)$$

obtained by using 3.26. On the other hand, if both dividers have the same phase error, the noise figure can be simplified as

$$F_d \approx F_m + 4 \left( r_n + F_m \frac{|\Gamma_i|^2}{4} (1 - \theta^2) \right) \frac{|\Gamma_s|^2}{1 - |\Gamma_s|^2} \quad (3.34)$$

that makes the noise figure degradation negligible. Fig. 3.11 shows the effect of the phase imbalance on the noise figure. If there is the same amount of phase imbalance canceling each other for the input and output dividers, the noise figure degradation is negligible as we proved in 3.34. However, if only the input divider has the phase imbalance, then the degradation becomes more as the imbalance increases. A worse  $\Gamma_s$  value enhances the amount of degradation on the noise figure.

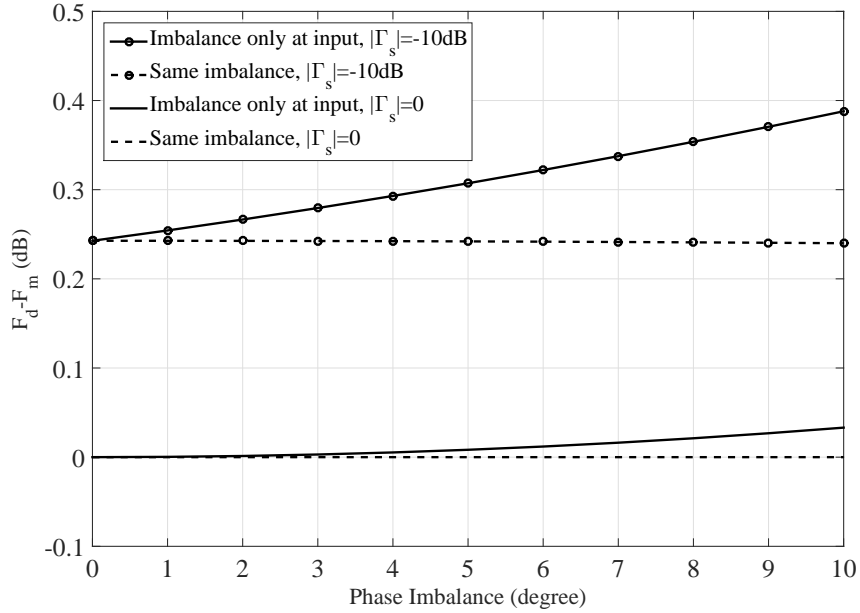


Figure 3.11: Noise figure degradation with respect to the phase imbalance. The amplifiers have  $|\Gamma_i|=-7$  dB,  $F_m=1$  dB,  $r_n = 0.1$  and  $\Gamma_o=0$ .

### 3.2.3 Non-zero $\Gamma_o$

In the previous analysis, we assumed that the optimal source impedance of the amplifier is zero. By using the noise wave approach, the effect of the non-zero  $\Gamma_o$  on the noise figure can be analytically found. For simplicity, assume that the input and the output dividers are ideal. So, with the help of the analysis given in section 3.1,

$$F_d = F_m + \frac{4(r_n M + F_m |\Gamma_i|^2 / 4) |\Gamma_s|^2}{1 - |\Gamma_s|^2}, \quad (3.35)$$

where

$$M = \frac{|\Gamma_o / \Gamma_s|^2 + |1 - \Gamma_i \Gamma_o|^2}{|1 + \Gamma_o|^2}. \quad (3.36)$$

We can recheck that, if  $\Gamma_o = 0$ , 3.35 will simplify to 3.25. Besides, if we rearrange 3.35 by adding and subtracting  $4r_n |\Gamma_o|^2 / |1 + \Gamma_o|^2$ , we can find the noise parameters of the balanced amplifier with a non-zero  $\Gamma_o$  as,

$$F_{md} = F_m + \frac{4r_n |\Gamma_o|^2}{|1 + \Gamma_o|^2}, \quad (3.37)$$

$$\Gamma_{od} = 0, \quad (3.38)$$

$$r_{nd} = r_n \frac{|\Gamma_o|^2 + |1 - \Gamma_i \Gamma_o|^2}{|1 + \Gamma_o|^2} + F_m \frac{|\Gamma_i|^2}{4}. \quad (3.39)$$

It is seen that, the minimum noise figure and noise resistance of the balanced amplifier are changed by additional terms which are the functions of  $\Gamma_o$ . For  $\Gamma_o = 0$ ,  $F_{md} = F_m$  and  $r_{nd} = r_n + F_m |\Gamma_i|^2 / 4$ . It's also important that, although the optimal source impedance of a single amplifier is non-zero, the optimal source impedance of the balanced amplifier is zero. It is consistent with the result obtained in 3.28 that,  $\Gamma_{od}$  directly depends on the input reflection coefficient of the input divider which is zero.

Table 3.1: Measured parameters for amplifiers  $A_1/A_2$ (GALI-84+) and  $A_3/A_4$  (PGA-103+) at 1.55 GHz.

Amp	$ \Gamma_i $ (dB)	$F_m$ (dB)	$r_n$
$A_1/A_2$	-14.4/ - 13.9	5.62/5.62	0.85/0.87
$A_3/A_4$	-16.7/ - 17.4	0.90/0.88	0.10/0.09

### 3.2.4 Experimental Results for Noise Figure

To verify the equations of the noise parameters and the noise figure degradation in a balanced amplifier experimentally, two pairs of amplifiers,  $A_1$ - $A_2$ ,  $A_3$ - $A_4$  are fabricated<sup>3</sup>. The inputs of the amplifiers are matched at 1.55 GHz to the optimal noise impedance ( $\Gamma_o = 0$ ) to get the noise figure of  $F_m$ . Table 3.1 lists the parameters measured using Keysight PNA-X N5242A Network Analyzer at 1.55 GHz. Two dividers (with intentionally poor return loss and isolation to see their effect more clearly) with an ohmic loss of 0.2 dB are manufactured. The dividers have  $|\Gamma_r|$  values of -11 dB ( $D_{11}$ - $D_{12}$ :  $D_1$ ) and -25 dB ( $D_{21}$ , $D_{22}$ :  $D_2$ ), while the  $|\Gamma_1|$ ,  $|\Gamma_2|$  and  $|I|$  have nearly the same value of -17 dB. The S-parameters of the dividers are plotted in Figs. 3.12 and 3.13 for the frequency range of 1.5–1.6 GHz.

Four balanced amplifiers using different combinations of dividers and amplifier pairs (see Fig. 3.14) are tried:  $B_1$  designed with  $A_1$ - $A_2$ ,  $B_3$  designed with  $A_3$ - $A_4$ , both using the divider  $D_1$ ;  $B_2$  designed with  $A_1$ - $A_2$ ,  $B_4$  designed with  $A_3$ - $A_4$  both using the divider  $D_2$ . The noise parameters of the balanced amplifiers are measured using Keysight PNA-X N5242A in the frequency range 1.5–1.6 GHz. The same parameters are calculated using (3.28) from the measured individual amplifier parameters. The comparisons are presented in Fig. 3.15 and Fig. 3.16 indicating a good agreement. The measured values of  $\Gamma_{od}$  are equal to the measured values of  $\Gamma_r^*$ , confirming our theory. From (3.28),  $\Gamma_{od}$  depends on only the input return loss of the divider. Since the impedance of the network analyzer is 50 ohm ( $\Gamma_s = 0$ ), the balanced amplifier using the divider with a better  $\Gamma_r$  ( $\Gamma_s$  is

<sup>3</sup>Mini-Circuits, NY 11235, USA, <http://www.minicircuits.com>

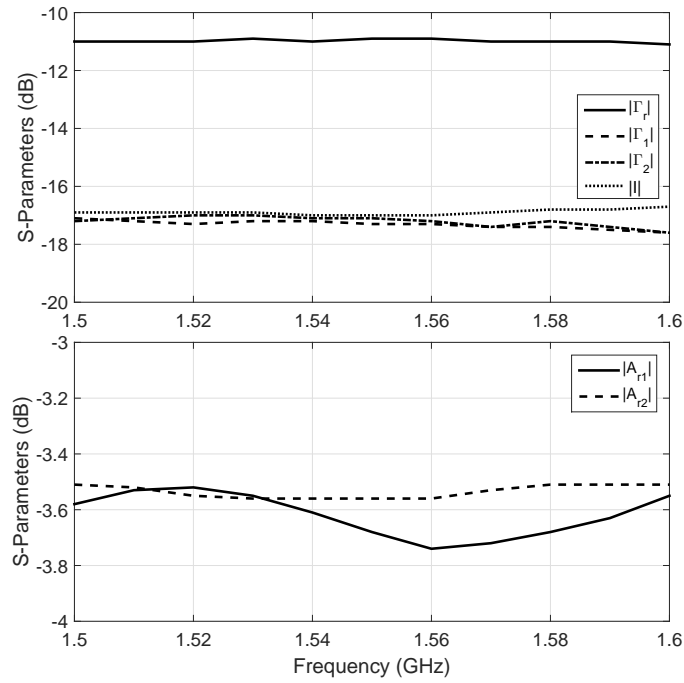


Figure 3.12: S-parameters of the  $D_1$  having poor  $|\Gamma_r|$  plotted with respect to the frequency.

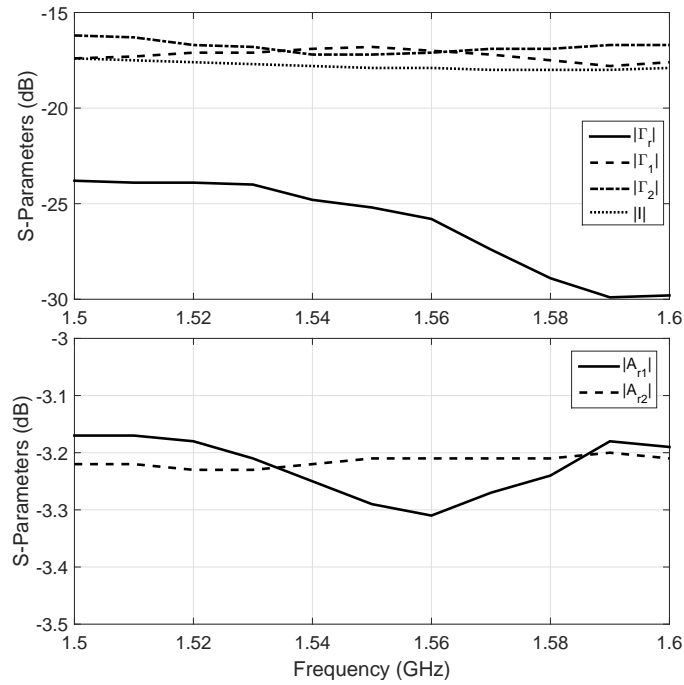


Figure 3.13: S-parameters of the  $D_2$  having good  $|\Gamma_r|$  plotted with respect to the frequency.

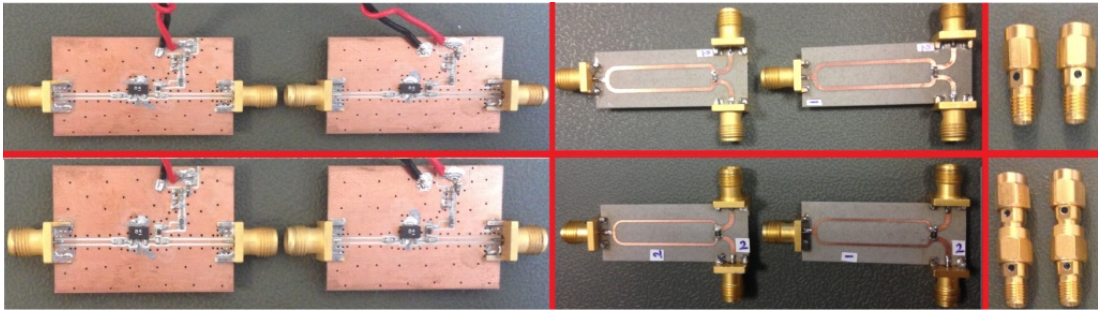


Figure 3.14: Photo of the amplifiers, divider pairs and SMA line extenders used to build balanced amplifiers.

close to  $\Gamma_{od}$ ) has a lower noise figure.

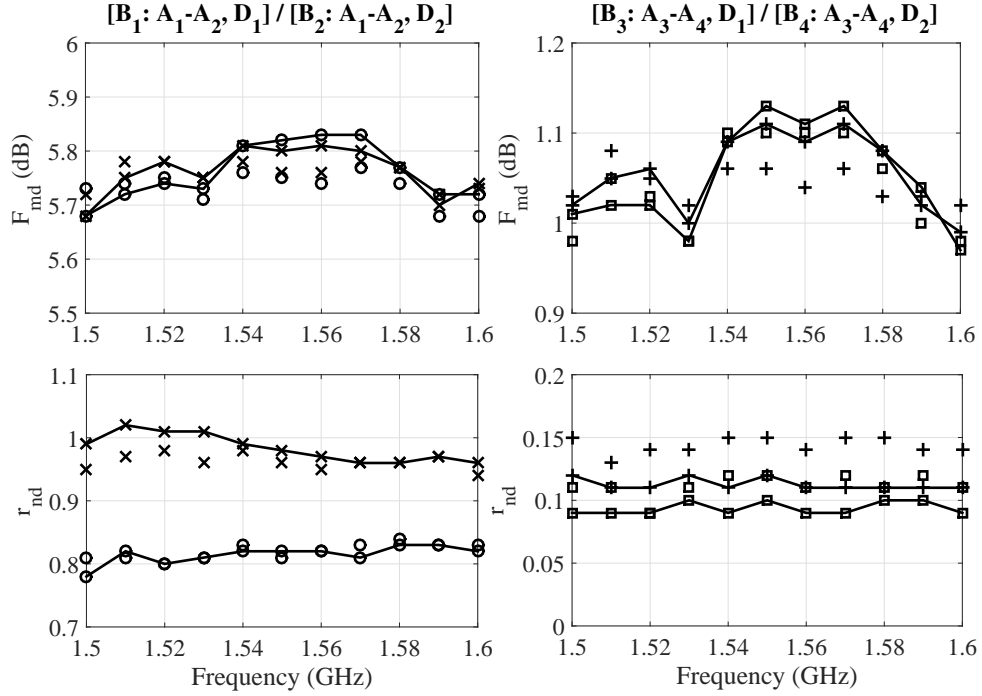


Figure 3.15: Calculated (solid) and measured (points)  $F_{md}$  and  $r_{nd}$  for the balanced amplifiers  $B_1$  (circle),  $B_2$  (cross),  $B_3$  (square) and  $B_4$  (plus). The graphs show the good agreement between the theoretical and measurement results.

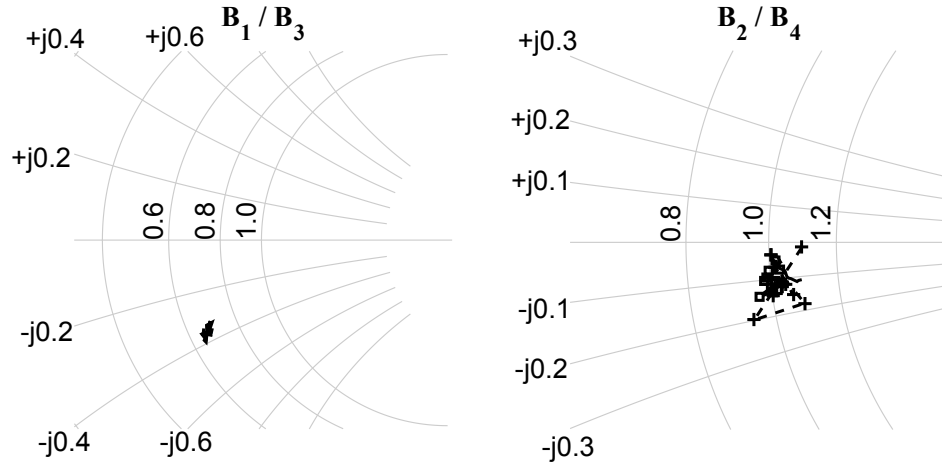


Figure 3.16: Calculated (solid) and measured (points)  $\Gamma_{od}$  for the balanced amplifiers on the Smith chart in the frequency range 1.5–1.6 GHz. The measured values of  $\Gamma_{od}$  are equal to the measured values of  $\Gamma_r^*$ , confirming our theory.



# Chapter 4

## Conclusion

We analyzed the total gain variation for balanced amplifiers using 2-way  $0^\circ$  dividers and  $90^\circ$  couplers. We obtained analytical expressions of the total variation in  $|S_{21}|$  for both balanced structures. The expressions indicate that the maximum gain variation is greater if  $90^\circ$  coupler is used in the balanced structure as opposed to a 2-way  $0^\circ$  divider for the same amplifier/divider parameters. We verified experimentally the analytical expressions we derived by designing a balanced amplifier and measuring the variation in the gain.

Furthermore, by using the noise wave approach, we found the output noise powers generated by each element of the balanced amplifier. Then, we analyzed the noise figure for a balanced amplifier and we provide approximate analytical expressions for the noise figure and noise parameters. While a balanced amplifier provides an input port with a high return loss, it degrades the noise parameters even when an ideal divider is used when  $|\Gamma_i|$  is non-zero. With an imperfect divider there is further degradation in the noise parameters. This degradation is not only from the ohmic loss of the divider, but also from its input return loss. While a typical phase imbalance in the divider does not cause a problem, an amplitude imbalance may degrade the noise figure further. Besides, for non-zero  $\Gamma_o$ , both the  $F_{md}$  and  $r_{nd}$  change dependent to  $\Gamma_o$  whereas  $\Gamma_{od}$  becomes 0. The presented graphs emphasize the need for a high performance input divider to limit the noise figure degradation.

# Bibliography

- [1] M. W. Pospieszalski, “On the noise parameters of isolator and receiver with isolator at the input,” *IEEE Trans. Microw. Theory Techn.*, vol. MTT-34, p. 451453, June 1986.
- [2] D. M. Pozar, *Microwave Engineering, 3rd ed.* New York: Wiley, 2005.
- [3] R. S. Engelbrecht and K. Kurokawa, “A wideband low noise L-band balanced transistor amplifier,” *Proc. IEEE*, vol. 53, pp. 237–247, Mar. 1965.
- [4] K. Kurokawa, “Design theory of balanced transistor amplifiers,” *Bell Syst. Tech. J.*, vol. 44, pp. 1675–1698, Oct. 1965.
- [5] S. Padin and G. G. Ortiz, “A cooled 1-2 ghz balanced hemt amplifier,” *IEEE Trans. Microw. Theory Techn.*, vol. 39, pp. 1239–1243, Jul. 1991.
- [6] C. C. Yang, B. L. Nelson, B. R. Allen, W. L. Jones, and J. B. Horton, “Cryogenic characteristics of wide-band pseudomorphic HEMT MMIC low-noise amplifiers,” *IEEE Trans. Microw. Theory Techn.*, vol. 41, pp. 992–997, Jul. 1993.
- [7] J. Jussila and P. Sivonen, “A 1.2-V highly linear balanced noise-cancelling LNA in 0.13- $\mu\text{m}$  CMOS,” *IEEE Journal of Solid-State Circuits*, vol. 43, pp. 579–587, Mar. 2008.
- [8] U. Schmid *et al.*, “Robust wideband LNA designs,” *EuMIC*, 2014.

- [9] J. Zhu and P. R. Kinget, “Frequency-translational quadrature-hybrid receivers for very-low-noise, frequency-agile, scalable inter-band carrier aggregation,” *IEEE Journal of Solid-State Circuits*, vol. 51, pp. 3137–3151, Dec. 2016.
- [10] P. V. Testa *et al.*, “A 210-GHz SiGe balanced amplifier for ultrawideband and low-voltage applications,” *IEEE Microw. Compon. Lett.*, vol. 27, pp. 287–289, Mar. 2017.
- [11] S. Seo, D. Pavlidis, and J. S. Moon, “Wideband balanced AlGaIn/GaN HEMT MMIC low noise amplifier,” *Electron. Lett.*, vol. 41, pp. 37–38, Aug. 2005.
- [12] W. R. Deal *et al.*, “Design and analysis of broadband dual-gate balanced low-noise amplifiers,” *IEEE J. Solid-State Circuits*, vol. 42, p. 21072115, Oct. 2007.
- [13] I. Malo-Gomez *et al.*, “Cryogenic hybrid coupler for ultra-low-noise radio astronomy balanced amplifiers,” *IEEE Trans. Microwave Theory Tech.*, vol. 57, p. 32393245, Dec. 2009.
- [14] S. C. Cripps, *RF Power Amplifiers for Wireless Communications, Second Edition*. Norwood, MA: Artech House, 2006.
- [15] K. Chang and C. Sun, “Millimeter-wave power-combining techniques,” *IEEE Trans. Microw. Theory Techn.*, vol. MTT-31, pp. 91–107, Feb. 1983.
- [16] S. D’Agostino and C. Paoloni, “Innovative power distributed amplifier using the Wilkinson combiner,” *IEE Proc. Microw. Antennas Propag.*, vol. 142, pp. 97–101, Apr. 1995.
- [17] P. J. Riemer, J. S. Humble, J. F. Prairie, J. D. Coker, B. A. Randal, B. K. Gilbert, and E. S. Daniel, “Ka-band SiGe HBT power amplifier for single-chip T/R module applications,” in *Proc. IEEE MTT-S Int. Microw. Symp. Dig.*, pp. 1071–1074, Jun. 2007.

- [18] S. Banba and H. Ogawa, "Small-sized MMIC amplifiers using thin dielectric layers," *IEEE Trans. Microw. Theory Techn.*, vol. 43, pp. 485–492, Mar. 1995.
- [19] A. E. Fathy, S. Lee, and D. Kalokitis, "A simplified design approach for radial power combiners," *IEEE Trans. Microw. Theory Techn.*, vol. 54, pp. 247–255, Jan. 2006.
- [20] C. Tseng and C. Chang, "Improvement of return loss bandwidth of balanced amplifier using metamaterial-based quadrature power splitters," *IEEE Microw. Compon. Lett.*, vol. 18, pp. 269–271, Apr. 2008.
- [21] R. L. Ernst, R. L. Camisa, and A. Presser, "Graceful degradation properties of matched N-Port power amplifier combiners," in *IEEE MTT-S Int. Microw. Symp. Dig.*, pp. 174–177, 1977.
- [22] T. T. Ha, "Microwave power combining and graceful degradation," *Proc. Inst. Elect. Eng.*, vol. 127, pp. 148–152, Jun. 1980.
- [23] A. A. Saleh, "Improving the graceful-degradation performance of combined power amplifiers," *IEEE Trans. Microw. Theory Techn.*, vol. MTT-28, pp. 1068–1070, Oct. 1980.
- [24] N. Picard, J. M. Denoual, D. Bourreau, and A. Peden, "Analysis of failure impact on microwave power combining," in *Proc. 39th Eur. Microw. Conf.*, pp. 898–901, Sep. 2009.
- [25] W.-C. Lee and T.-H. Chu, "Design and power performance measurement of a planar metamaterial power-combined amplifier," *IEEE Trans. Microw. Theory Techn.*, vol. 61, pp. 2414–2424, Jun. 2013.
- [26] H. L. Lee, D. Park, M. Lee, and J. Yu, "Reconfigurable 2x2 multi-port amplifier using switching mode hybrid matrices," *IEEE Microw. Compon. Lett.*, vol. 24, pp. 129–131, Feb. 2014.
- [27] M. S. Gupta, "Degradation of power combining efficiency due to variability among signal sources," *IEEE Trans. Microw. Theory Techn.*, vol. 40, pp. 1031–1034, May 1992.

- [28] K. W. Eccleston, “Consequences of port mismatch and finite isolation on power combining,” in *Conf. Proc. Singapore ICCS '94*, vol. 1, pp. 246–250, Nov. 1994.
- [29] A. Peden, J. M. Denoual, B. Della, J. P. Fraysse, L. Lapierre, and G. Soubercaze-Pun, “Phase compensation technique in a radial divider/combiner structure,” in *Proc. 40th Eur. Microw. Conf.*, pp. 176 – 179, Sep. 2010.
- [30] M. S. Gupta, “Power combining efficiency and its optimization,” *IEE Proc. H Microw. Antennas Propag.*, vol. 139, pp. 233–238, Jun. 1992.
- [31] Z. Galani, J. L. Lampen, and S. J. Temple, “Single-frequency analysis of radial and planar amplifier combiner circuits,” *IEEE Trans. Microw. Theory Techn.*, vol. 29, pp. 642–654, Jul. 1981.
- [32] A. R. Kerr, “On the noise properties of balanced amplifiers,” *IEEE Microw. Guided Wave Lett.*, vol. 8, pp. 390–392, Nov. 1998.
- [33] A. A. Abidi and J. C. Leete, “De-embedding the noise figure of differential amplifiers,” *IEEE Journal of Solid-State Circuits*, vol. 34, pp. 882–885, Jun 1999.
- [34] O. Garcia-Perez *et al.*, “Noise-figure measurement of differential amplifiers using non-ideal baluns,” *IEEE Trans. Microw. Theory Techn.*, vol. 59, pp. 1658–1664, Jun 2011.
- [35] Agilent Technologies, 2001. Application Note 64-1C: “Fundamentals of RF and Microwave Power Measurements”.
- [36] R. Gilmore and L. Besser, *Practical RF Circuit Design for Modern Wireless Systems: Active Circuits and Systems*, vol. II. Norwood, MA:, 2003.
- [37] A. A. Coskun and A. Atalar, “Noise figure degradation in balanced amplifiers,” *IEEE Microw. Compon. Lett.*, 2017, in press.
- [38] V. Tas and A. Atalar, “An optimized isolation network for the Wilkinson divider,” *IEEE Trans. Microw. Theory Techn.*, vol. 62, Dec. 2014.

- [39] S. Mason, "Feedback theory: some properties of signal flow graphs," *Proc. of IRE*, vol. 41, pp. 1144–1156, 1953.
- [40] R. Walton. <http://www.mathworks.com/matlabcentral/fileexchange/22-mason-m>. mason.m script for MATLAB.
- [41] R. P. Meys, "A wave approach to noise properties of linear microwave devices," *IEEE Trans. Microw. Theory Techn.*, vol. 26, pp. 34–37, Jan. 1978.
- [42] P. Penfield, "Wave representation of amplifier noise," *IRE Trans Circuit Theory*, vol. CT-9, pp. 83–84, Mar 1962.
- [43] H. Hillbrand and P. Russer, "A wave approach to noise properties of linear microwave devices," *IEEE Trans. Circuits Systems.*, vol. 23, pp. 235–238, Apr. 1976.
- [44] R. P. Hecken, "Analysis of linear noisy two-ports using scattering waves," *IEEE Trans. Microw. Theory Techn.*, vol. MTT-29, pp. 997–1004, Oct. 1981.
- [45] V. Rizzoli and A. . Lipparini, "Computer-aided noise analysis of linear multiport networks of arbitrary topology," *IEEE Trans. Microw. Theory Techn.*, vol. MTT-33, pp. 1507–1512, Dec. 1985.
- [46] N. G. Kanaglekar, R. E. McIntosh, and W. E. Bryant, "Wave analysis of noise in interconnected multiport networks," *IEEE Trans. Microw. Theory Techn.*, vol. MTT-35, pp. 112–115, Feb. 1987.
- [47] S. W. Wedge and D. B. Ruthledge, "Wave techniques for noise modeling and measurement," *IEEE Trans. Microw. Theory Techn.*, vol. 40, pp. 2004–2012, Nov. 1992.
- [48] J. A. Dobrowolski, "A CAD-Oriented method for noise figure computation of two-ports with any internal topology," *IEEE Trans. Microw. Theory Techn.*, vol. 37, Jan. 1989.
- [49] R. Q. Lane, "The determination of device noise parameters," *Proc. IEEE*, vol. 57, pp. 1461–1462, Aug. 1969.